11

Quantum Mechanics Design of Two Photon Processes Based Solar Cells

Abdennaceur Karoui and Ara Kechiantz
Photovoltaic Nanotechnology and Nanosensors Laboratory,
Shaw University, Department of Natural Sciences and Mathematics
USA

1. Introduction

The photoelectric effect has been utilized in a wide range of optoelectronic sensors and solar energy conversion devices. To respond to today's colossal energy demand there is a need for doing better than using this effect via the utilization of simple semiconductor homojunction based devices, since such structures cannot use all photons available for conversion into electricity. Actually, it is the inefficient response of the material to the various solar photons and the behaviour of photo-generated carriers that bar photovoltaic (PV) cells from fully harvesting the solar energy impinging on its surface. It is well known that there is no semiconductor that can be deployed for making a simple and low cost p-junction based solar cell that converts the entire solar spectrum. Hence, the development of efficient photovoltaic devices has been going through various technology pathways, one of which has led to a variety of multi-junction and cell stacks, i.e., tandem cells; each sub-cell is dedicated to converting a portion of the solar spectrum. Moreover, the conventionally chosen three sub-cell tandem scheme is being extended to stacks with larger number of sub-cells, regardless of the viability of the production technology.

During the last five decades, several theoretical PV energy conversion efficiency thresholds have been established, each being for one type of PV device design. However, none has been reached in spite of the deployed tremendous efforts; the implementation turns out to be challenged by some specific constrains. High efficiencies attained thus far incorporated advances in material refinement, sophisticated cell design, state of the art fabrication technologies, and more importantly a relatively good understanding of the complicated and intertwined physics of charge carrier generation, recombination, and transport. However, for making new generation of high efficiency solar cells, new physics and technology paradigms have to be discovered. Current barriers to high conversion efficiencies are due to current understanding of the physics of photoelectric effect and related phenomena. Breaking those barriers, which would impact photovoltaic technologies, needs refinement of the physics of photoelectric effect with consideration of new materials and new device designs. For instance, development of "ideal" third generation solar cells requires understanding of the early stage of light-matter interaction mechanisms that occur at the nanoscale domains and the related quantum effects. Actually, the improved understanding of these phenomena is repositioning the used linear photoelectric effect occurring in homogenous and continuous planar shallow structure to one that occurs in a volumic

structure with nanoscale features. These induce rather non-linear effects entangled with quantum effects. Additionally, a precise account of the charge carriers within the cell has to be accomplished. Inclusive to that need are (i) the improvement of photon absorption over a wider spectral range by adequately engineering the semiconductor optical properties, (ii) immediate use of photo-generated electron-hole pairs, (iii) the local charge carrier separation and collection, and (iv) transport to remote electric contacts; all of which should be studied at the nanoscale level.

As the quantum processes and the discrete nature of electron transitions are fundamental to photoelectric effect, this chapter focuses on (i) reviewing light-matter interaction quantum processes that are directly or indirectly involved in the photoelectric effect, (ii) discussing those that are useful for third generation PV cells, and (iii) highlighting recent research results by the author. Fundamental quantum processes initiated by photon absorption and their contribution to the solar energy conversion will be reviewed in connection to the electron energy structure of the absorber material. New ideas relevant to absorbers within third generation solar cells will be presented. The nature of light-electron interaction is scrutinized and elementary processes of light absorption, atom excitation, atom ionization, photon excess energy dissipation, emitted charge carrier pairs, carrier transport and/or recombination are discussed in terms of exchanged energy, momentum transfer and photon-electron interactions in nanometer and atomic scales. We will assess the major losses that have quantum bearings and elucidate their effects on third generation solar cells. We will present a novel solution, which employs two-photon absorption . This is a cooperative non-linear process that occurs in two sequential stages. It employs two photons, that have an energy lower than the semiconductor bandgap. The two-photon absorption produces a net optical transition between valence and conduction bands through an Intermediary energy Band (IB) laying within the bandgap of the host material. Photoelectric effect employing two photon processes is a research area of strong scientific interest that drives science and technology research towards making new solar cells among third generation. We will delve into the reasons as to why the two-photon absorption is still not optimally used to make efficient solar cells. In single-photon absorption by indirect semiconductors, phonon cascades are usually involved. The energy and momentum conservation during such photon absorption sequence obligates one to look at the thermodynamics of a solar device and the factors of thermalization, a major effect that reduces the quantum efficiency of the photoelectric effect. The processes and factors controlling the two-photon absorption, which involves virtual or real intermediate states, are presented. Next, quantum phenomenon involved in nanostructured PV device operation is electron tunnelling through energy barriers that spatially separates confined electronic states.

The second part of the chapter will present modelling of new materials that are designed to promote two photon absorption processes in solar cells. The studied system is a circular chain of QDs embedded in nanostructured material, a set of QD chains attached to the inner walls of pores in porous silicon (Karoui & Kechiantz, 2011). Confinement of electron wave-functions breaks the initially continuous electron energy spectrum into discrete energy levels. There are some apparent differences of this effect in QDs and the well understood atom systems, although the underlying physics is the same. We will discuss these differences in relation to their relevance to the studied nanostructured PV material. It is argued that while decaying beyond the potential barrier associated with the QD-host material interface, electron wave-functions penetrate into the host material, which enables overlapping of confined electron wave-functions. We will show how a wave-function that

spills over the interface enables creation of energy bands in the host solid out of the energy levels of the QDs embedded in the nanostructured PV system.
It should be noted that the intention of this chapter is neither to report on a mere quantum mechanics calculation, nor to give an account on photoelectric applications, but to bridge the gap between the physical quantum processes driving the photoelectric effect. This has been mostly over simplified in conventional PV applications. It has become known that modern PV device engineering focuses on increasing efficiency of those devices thereby targeting the 65% limit defined by Luque and Marti. This high goal appears to require the use of nanostructured semiconductor systems. In that context, the optoelectronic quantum processes can no longer be neglected. Therefore, to obtain the most out of the photoelectric effect and overcome the new challenge of 65% conversion efficiency, one needs to deepen the physics knowledge on these processes and put them into the context of real material systems and devices. Detailed experimental and theoretical studies related to those quantum processes occurring in the presented novel PV design will be published by the author of this chapter.

2. Quantum mechanics aspects of solar energy conversion

2.1 Interaction photon-solids

2.1.1 The energy-moment space in semiconductors

The electron energy-momentum *(***E-k***)* relationship is well known to be fundamental for obtaining the physical properties of solids. It governs many optical and electronic related phenomena in solids, in particular photoelectric related processes. This relationship is very sensitive to the periodicity of the crystal potential in which the electron propagates. The *(***E-k***)* relationship is obtained in the one-electron approximation by solving the Schrodinger equation for electron in effective periodic crystal field. The crystal periodic field renormalizes the electron momentum and defines a new complex energy-momentum *(***E-k***)* relationship, given in *Brillouin zone,* that essentially differs from the simple parabolic energy-momentum relationship shown in Figure 1(a) for free electron with m_e the electron mass in the free space. Figure 1(b) and (c) show the very well-known energy-momentum for Si and GaAs, respectively, to remind the complexity of the energy band structure of solids. The *(***E-k***)* relationship is a multifold function of momentum, since the same momentum refers to different electron energies. The *(***E-k***)* is chiefly parabolic near the crystal lattice symmetry points $(\Gamma, L, X, ...)$ only, but the concavity variation is characteristic, in a first order approximation, of crystal symmetry in these points and the band energy variation in the vicinity of the considered point. This variation commensurate with the *electron effective mass*.
Because *Pauli Exclusion principle* limits the occupation of the same energy-momentum-spin electronic state to one electron, some energy bands are completely filled with electrons while others are either empty or partially filled in the vicinity of the symmetry points as shown in Figure 1(b) and (c). Like free electrons, in the vicinity of the symmetry points, the *energy and* to be conserved even though the interaction with other particles, in the solid, can be very strong and can occur in stages. All interactions are bound by the complex *(***E-k)** relation.
Changes in electron energy-momentum *(***E-k***)* relationship in solids are essentially *quantum mechanical effects*, and can be found by solving the Schrödinger Equation.

2.1.2 Absorption and emission, direct and indirect electron transitions

Engineering semiconductors that fully absorb the entire energy of incident photons over the entire solar spectrum constitute an ambitious goal. This can be at best approached by

nanotechnology and used for by third generation PV cells. To better utilize the photoelectric effect, solid state *fundamental processes* must be addressed individually at various time, space, and energy scales. These basically include *photon absorption* and *emission* and subsequent *electron-hole generation, recombination, separation,* and *collection*. Additionally, other processes such as the involvement of phonon cascades, surface plasmons and polarons,… must be taken into account for nanoscale investigations, Single or cascade of such processes move electrons from one energy level to another, which brakes the equilibrium of the electronic system and leads to a cascade of other processes that ultimately bring the system back to its thermodynamic equilibrium.

The blue arrows and red curly-arrows in Figure 1(b) and (c) illustrate photon absorption resulting in the electron transfer from the valence band into the conduction band. The reverse process is the electron transfer from the conduction band into the valence band, which results in photon emission (illustrated by green arrows and red curly-arrows in Figure 1(b) and (c)).

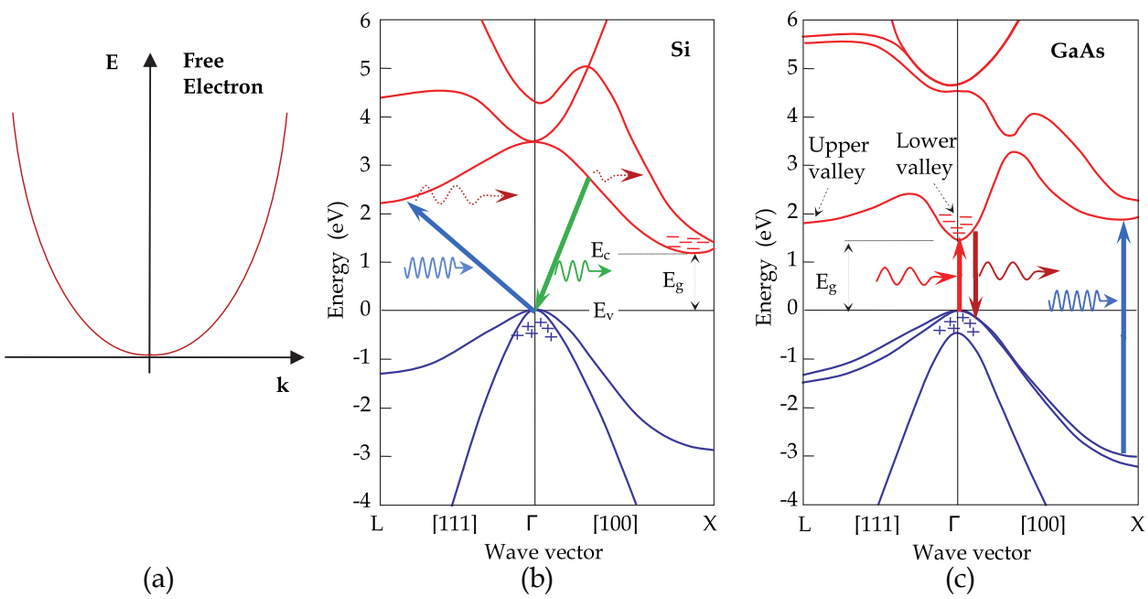

Fig. 1. Electron energy-momentum (E-k) relationship and electron transitions in: a) the free space; b) the indirect bandgap silicon; c) the direct bandgap GaAs.

Since photon momentum is very small compared to that of electron, the momentum conservation allows only electron transitions between energy levels with practically no electron momentum variation (thus the same wave vector) in the Brillouin zone. The vertical blue and green arrows display such *direct electron transitions* in Figure 1(c) for a direct bandgap semiconductor, here GaAs. When there is not an empty state that enables photon induced electron transition with momentum conservation, phonon assistance is required to ensure momentum conservation. *Indirect electron transitions* must involve both phonon and photon, as illustrated in Figure 1(b), where dotted curly-arrows represent phonons.

2.1.3 Radiative and non-radiative recombination

Charge Carrier Recombination is the electron-hole annihilation in semiconductors, where the electron returns from the high-energy electronic state to an empty low-energy electronic

state, for instance from the conduction band to the valence band R*adiative recombination* results in photon emission with conservation of both energy and momentum. However, recombination can also happen without photon assistance, which is known as *non-radiative recombination*. For instance, phonon can assist recombination through impurity related levels within the semiconductor bandgap.

Recombination is very important in photovoltaics and for other optoelectronic devices as well. While photon absorption generates photocurrent, electron-hole recombination suppresses the photocurrent and generates dark current in these devices. Both absorption and recombination processes may become dominant and even complex in low cost photovoltaic materials, where a wide range of defects usually are tolerated, and in semiconductor structures when multi-particle processes like Auger recombination assist electron relaxation.

2.1.4 Shockley–Read–Hall (SRH) recombination

Single and cluster impurities in the crystal either in interstitial or in lattice positions promote electron transition between bands passes through the energy level created within the band gap. During transition of charge carriers from valence band to conduction band, and vice-versa, the carriers take available states and most often those created by impurities. In satisfying the energy and momentum conservation across the entire process, the impurity state can absorb differences in momentum between the carriers. The process of generation and recombination via impurity levels is the dominant in indirect bandgap materials, such as silicon. This process can also be significantly important and dominate the charge carrier dynamics in direct bandgap materials particularly for very low carrier densities. The excess energy is dissipated in the form of lattice vibrations (absorbed phonon by the material give away their energy in the form of thermal energy). Impurities and crystal point defects and clusters create energy levels within the band gap. Figure 2 shows the known energy levels in silicon (Sze & Irvin, 1968) generated by metal impurities and crystal point defects. Light elements and neighbors to the periodic table fourth column mostly induce shallow levels, which are used beneficially as dopants, whereas transition metals for instance induce deep level traps. The latter actively participate in non-radiative carrier recombination and thus are detrimental charge carriers killers.

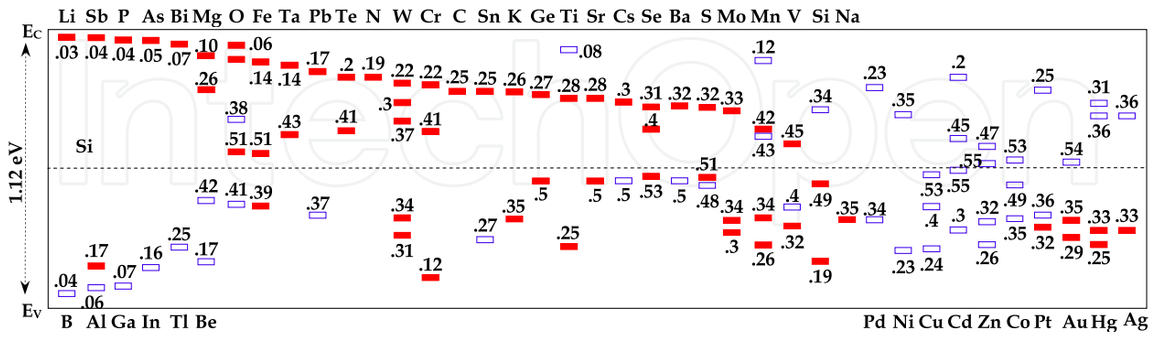

Fig. 2. Discrete energy levels of different impurities in Si energy bandgap. (Sze & Irvin, 1968)

2.1.5 Auger recombination

This type of recombination contributes to the loss of electrons promoted to the conduction band by photon absorption. Under certain conditions this recombination becomes dominant thereby degrading the overall conversion efficiency of PV cells and photo-sensors.

Auger recombination is a non-radiative process that involves three mobile carriers two of which recombine and while vanishing they transfer their energy to a third carrier, the latter will continue to reside in the same band as a bound electron. Figure 4 illustrates the Auger recombination of photo-generated holes in p-type doped Si. Auger recombination process is controlled by majority carriers (here holes) since the recombination rate is proportional to np^2, where n and p are respectively the electron and hole concentrations. The energy transferred to the third carrier increases its energy without ascension to a higher energy band. The stored energy by the third carrier is then lost to thermal vibrations (phonons). This process is fast and involves three-particle interaction, the third is involved at a high-energy unstable state. The process is effective in non-equilibrium conditions, when the carrier density is very high, that is either in heavily doped semiconductor or under high injection levels. The green arrow in Figure 3 (b) represents the electron-hole annihilation while the red dashed arrow shows the energy transferred to another electron in the valence band. The blue arrow displays electron transition to a higher energy state in the valence band, which generates a "hot" hole. The readiness of the third particle for Auger Recombination makes the probability of this process rather low. The probability being proportional to np^2, as stated above in the case of p-type semiconductor, shows that Auger recombination rate swiftly grows with carrier density. This feature makes the Auger recombination a determinant factor in heavily doped solar cells, in particular in the device active zone and the surface as well as under concentrated sunlight irradiation when the density of injected or generated carriers is very large (Sinto & Swanson , 1987). For instance, when the density of photo-carriers is above $10^{18} cm^{-3}$ (Dziewior & Shmid, 1977, Svantesson & Nilsson, 1979). Auger process becomes very effective and dominates the recombination rate in high quality silicon solar cells (Green, 1984), which achieved the highest records of conversion efficiencies , and more as the cell efficiency is increased. Hence, device designs that alleviate Auger recombination at surface and interfaces must be thought out, particularly for concentration solar cells.

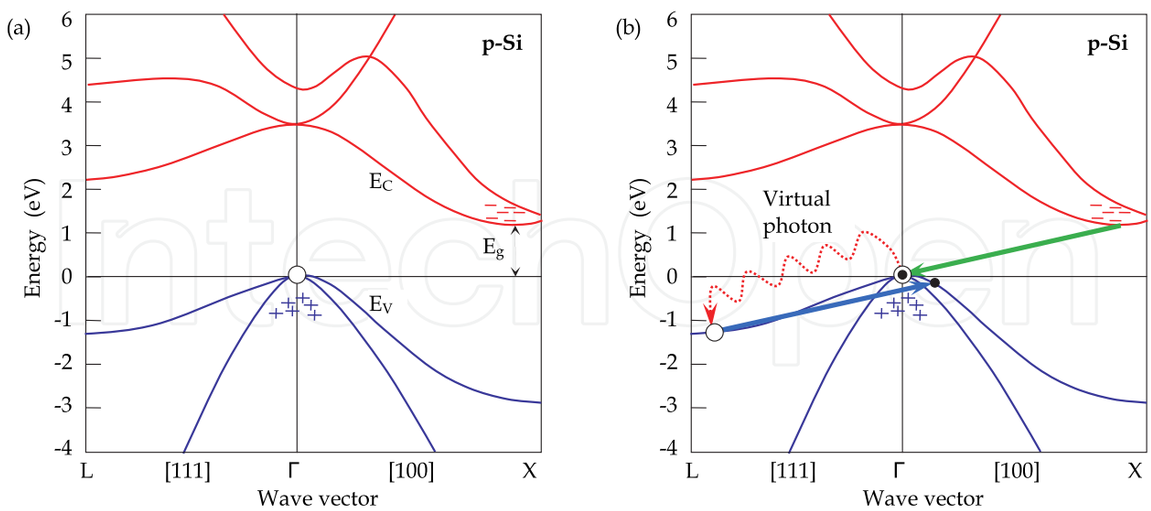

Fig. 3. Photo-generated holes in p-type Si (a), and Auger recombination of that hole (b).

2.2 Major quantum energy losses during carrier photo-generation and transport

For developing high efficiency PV devices one must find new approaches for absorbing the entire energy of incident photons, preventing internal losses, and collecting all produced

electrons. It is well known that there is a slate of energy losses inside and outside the device and the major internal losses have quantum origin. Hence, during the past two decades quantum mechanics has been extensively used for devising new generation of solar cells that minimize those losses. For that purpose, fundamental optoelectronic processes in semiconductors have been revisited aiming at fully exploiting the photon energy available in the solar spectrum as well as the handling of generated charge carriers in the PV devices. As we investigate the photoelectric effect at the nanoscale level, the generation and transport of charge carriers are looked at in details with the associated quantum effects.

2.2.1 Energy excess of photo-generated electrons, and thermalization

The fundamental solid state physics mechanisms that are responsible for energy losses in solar cell are shown in Fig. 4. The internal losses are basically due to the due to the "misfits" of energy-wavevector of incident photons with the electronic band structure characteristic of the material used to make the PV device. The problem is further aggravated as the misfit extends over the entire solar spectrum and thus difficult to correct. Radiative and non-radiative electron transitions between electronic states steadily take place along electron diffusion paths towards the p-n junction. The photoelectron intra-band relaxation processes, which involve thermal photons and phonons, become abundant as the electronic levels within conduction and valence energy bands become dense. Interactions of the material with the photons impinging the PV device surface involves extracted electrons, intermittently produced photons, and phonons, all of which occur via a cascade of radiative and non-radiative intra-band transitions that causes electron and hole thermalization in conduction and valence bands, respectively.

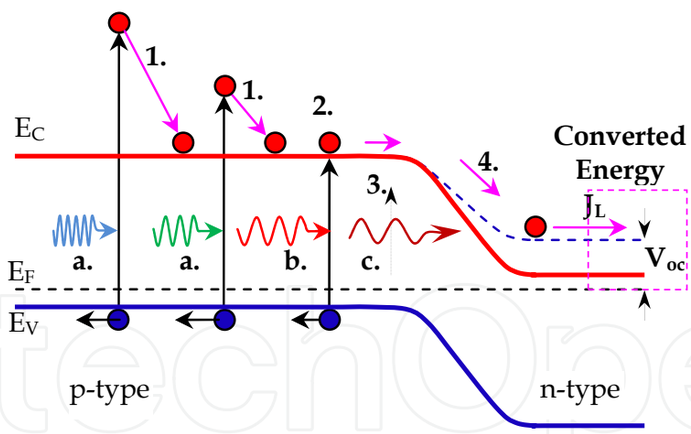

Fig. 4. Photoelectron excess energy leading to energy loss processes in a solar cell made of one p-n-junction; a. High energy photon absorbed, b. photons that have energy exactly equal to the absorber bandgap, c. low energy photons that are usually transmitted, 1. Thermalization via intraband transitions, 2. Absorption without loss, 3. Electronic energy loss during transition through depletion region (i.e., separation of e-h pair).

The three main fundamental processes of energy loss in solar energy conversion devices are schematically shown in Fig. 4. Photon absorption (a. and b. photons) usually produces electrons (electrons of type 1. or 2.) whose energy is larger than or equal to the energy they contribute into the electricity generated by the solar cell. Because the photoelectrons (1.) are in a non-equilibrium thermodynamic state with the electronic system and the crystal lattice,

they swiftly lose the excess energy through thermalization in intra-band inelastic scattering and collision processes with equilibrium electrons and phonons. The arrows attached to electrons labeled (1.) in Fig. 4 illustrate such intra-band electron relaxation processes (thermalization). Also there is a wide range of low-energy solar photons (pin pointed with the arrow labeled (3.) that do not have enough energy for transferring electrons from the valence band into the conduction band; these photons are conventionally transmitted through the material. However, low energy photons (c.) can still promote transitions of type (3.) through levels in the bandgap or participate in two photon absorption mechanism.
Because photoelectron generation uses less than the absorbed energy, intra-band loss mechanisms are unavoidable. After intra-band thermalization the photo-generated electron still retains more energy than what it uses in contributing to the output electricity. The photoelectron loses the difference of these energies during electron-hole separation, shown in Fig. 4 by the arrow labeled (4.), while transiting through the space charge region.
Figure 5 elucidates the impact of the internal losses using the AM1.5 solar irradiance impinging a silicon PV device. The usable energy under Shockley-Queisser limit is 31% of the incident light over the entire spectrum. The convertible energy amount is in regions (1.) and (2.) of Figure 4, which are the result of the effective absorption corresponding to (1.) and (2.). Likewise the converted amount by the state of the art silicon cell is 25% occurs in the same region of the spectrum. High energy photons in the Near-UV-Vis are absorbed at the material surface leading to a high recombination rate at the surface, and a significant loss

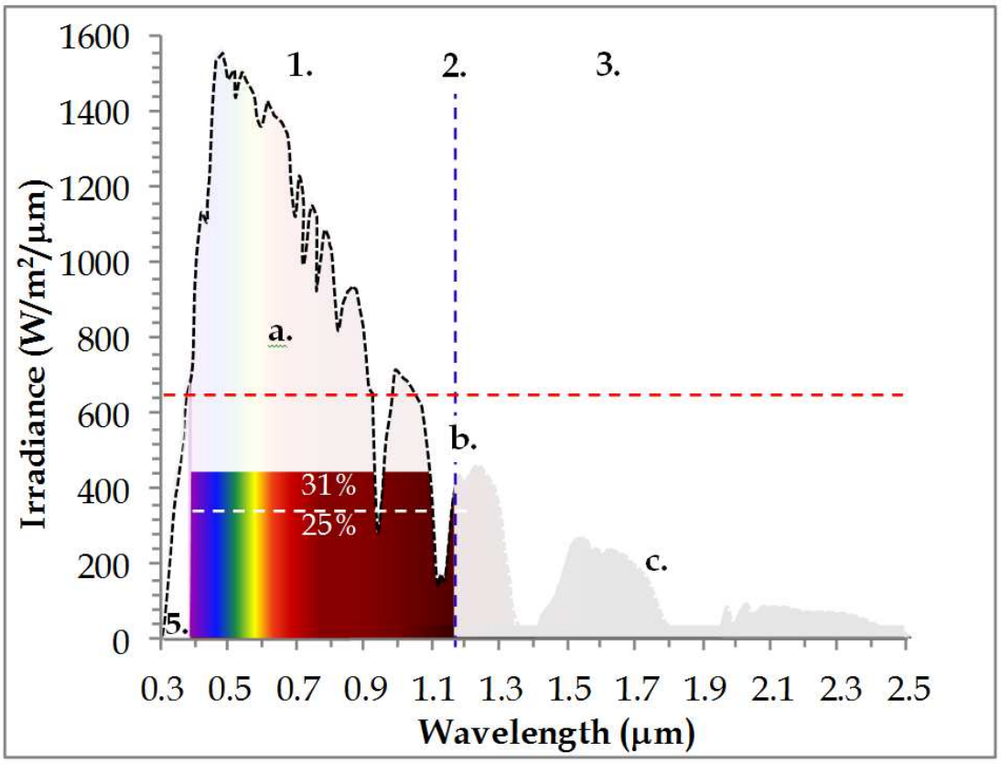

Fig. 5. Solar energy density as a function of the wavelength (AM1.5). Portions that cannot be converted by silicon single p-n homojunction solar cell is represented by greyed areas (1.), for photons that have energy lower than the bandgap, and (2.) for high energy photons, as a result of losses at the level of photon-solid interactions.

labeled (5.) in Fig. 4, this is evaluated to about 8%. Surface passivation has been used to reduce the surface recombination. These loss mechanisms result in a sizable amount of solar energy that cannot be converted in electricity in conventional single p-n-junction solar cells. several energy losses that do not have a quantum origin are also significant and undesirable but difficult to avoid. These are out of the scope of this chapter; nevertheless, it is useful to quickly overview them. Let's start with light reflection at the solar cell surface. Silicon reflectance reaches 31% in the visible range and more than 50% in the UV. Methods have been developed to reduce such losses, which consist in increasing the optical path at the surface by engaging a multiple reflection process. Silicon surface texture, nitrogen annealed and etched silicon (Karoui & Zhang, 2002), and sprayed porous silicon proved to be effective and low cost methods for reducing reflection losses. However, a non-resolvable loss by reflection remains, this is labeled in Fig. 5; and is evaluated to about 8% of the total incident energy.

The second loss stems from the emission of blackbody radiation by solar cells. The equilibrium temperature of a cell in operation leads to blackbody radiation emission. The temperature baseline is that of the surrounding. As the temperature of the cell increases during absorption of sunlight, the cell blackbody radiation increases and ultimately attains thermodynamic equilibrium with the incident radiation, leading to a temperature roughly between 80 and 95°C. The blackbody emitted radiation energy is lost to the ambient and thus cannot be converted to electricity by the cell. The loss by silicon cell via blackbody radiation can reach 70-80% incoming solar radiation energy.

The third category of loss is accidental. It arises when dissipation of electric energy from a PV cell array into low performing cells occurs. In this case the energy is dissipated within such cells in thermal form, which increases the temperature of the cell and thus the blackbody radiation. Henceforth, the associated blackbody loss is increased. Such loss is referred to as hot spot within a cell array. It leads the PV cell to operate at lower conversion efficiency or possibly to a catastrophic breakdown of the cell and the cell array.

2.2.2 Phonon assisted electron transitions and phonon bottleneck effect limiting charge carrier recombination in quantum dots

Phonon quantum energy is very small relative to semiconductor energy bandgap. This makes phonon assistance in electron interband transitions of in direct and ideal semiconductors likely, because of energy conservation. However, in real life semiconductors, decorated extended defects (e.g., dislocations,...) *single and clusters of* point defects (i.e., dissolved impurities, vacancies, self-interstitials,…) spread in the bulk and at the surface generate states and energy levels within energy bandgap. These energy levels are discrete and spatially localized in such non-ideal semiconductors. Both thermal photons and phonons can assist photon initiated electron inter-band transitions between such levels if energy difference between initial and final levels is small and the separation between these defects is low such it prevents any screening. Moreover, cascades of alternating phonon assisting and tunneling electron transitions can result in non-radiative inter-band electron-hole recombination.

Impurities, point defects, crystalline extended defects and their interactions have been assessed during the last three decades. In that respect, silicon is probably the most diagnosed semiconductor. For cost reasons, conventionally used photovoltaic materials are of much lower quality than microelectronic and optoelectronic materials. Acceptable energy level concentrations, and impurity states have been the focus for both academia and photovoltaic industry. Sufficiently efficient silicon solar cells have shown a certain tolerance

margin for impurities and charge carrier lifetime killers in the bulk and at the surface and have defined the baseline for low cost material growth technologies. In such materials non-radiative recombinations are dominant.

Intensity of non-radiative recombination increases with the defect electronic density of states associated with precipitates, decorated dislocations, vacancies, the hardly controllable dissolved impurities (in interstitial or substitution sites) etc., both in the bulk material and at the surface. Radiative inter-band transitions are only possible in solar cells made from ultra-clean materials. Shockley and Queisser have applied this property of clean semiconductors for evaluating limiting conversion efficiency in the best conventional one-junction solar cell (Shockley & Queisser , 1961). More recently, Luque and Marti have used the same property of clean semiconductors for evaluating the utmost conversion efficiency limits of IB solar cells (Luque & Marti, 1997). This is discussed in more details in the following sections.

Consecutive emissions of optical phonons is the main mechanism of photoelectron thermalization. The energy of an optical phonon in silicon is roughly about $50\ meV$. The characteristic time of such intra-band relaxation is about $10^{-12}s$ for photoelectrons in conventional solar cells. However, in dye or quantum dot (QD) sensitized solar cells, the relaxation process of photoelectrons may become slower. Such cells exploit the sensitizer discrete energy levels to enable additional photoelectron generation in the host material. The reduction of photoelectron relaxation, known as the "*phonon bottleneck*" effect in QDs, results from the lack of optical phonons that match separation of discrete energy levels in QDs (Guyot-Sionnest et al., 1999; Sun et al., 2006). The "phonon bottleneck" could be favorable for photovoltaic devices like solar cells and infrared and terahertz photodetectors operating at room temperature (Zibik et al, 2009) since radiative transitions dominate photoelectron relaxation in such QDs.

2.3 Solar energy conversion limits

2.3.1 Limiting factors for photon conversions and device inherent losses

It is important to contain the photoelectric efficiency under certain conversion limit. This essentially depends on the way the photoelectric effect is exploited and hence the device design and the type of used material. Furthermore, fabrication technologies involve detrimental factors to the exploitation of the photoelectric effect. The various fundamental limits for photon energy conversion will be debated, namely those of thermodynamics origin, detailed balance limit defined by Shockley and Queisser, and the new limit defined by Luke and Marti. The quantum mechanics based discussion will focus on the generation of charge carrier pairs as well as their recombination and how the photon energy can be better used to increase the quantum efficiency of PV devices. Electronic confinement in nanofeatures have become essential for third generation solar cells, thus needs extensive clarification. We will look at how the confinement affects light absorption and the overall conductivity, as these are key matters for high efficiency solar cells.

2.3.2 Photon recycling through optical and electronic transition cascades

The "photon recycling" terminology refers to transformation dynamics of absorbed photon-mode-fluxes through photovoltaic and optical sensor devices. Energetic photon generates electron-hole pair, which in turn produces new photon after the pair recombines radiatively. Because the new photon has energy above or equal to the band gap, it can create another electron-hole pair by re-absorption elsewhere in the cell, and so on and so forth. The "recycled photon" looks like a "virtual photon" in Feynman diagrams. Similar diagrams for

photon-solid interactions relevant to photovoltaics and "photon recycling" processes are presented in Figure 6, where:

- the dashed curled line represents the "photon recycling" process,
- the light blue and green arrows are incoming absorbed photons and the orange and dark blue are emitted photons exiting the PV device,
- CBC and VBC are contacts to conduction and valence bands, respectively, and
- the solid and the dashed brown double-line arrows represent the electron and hole currents, respectively.

At the end of recycling one can obtain one of the following mechanisms: a) incoming photon yields photocurrent; b) electron injected from a contact yields dark current and another photon emission; c) incoming photon causes emission of another photon, with a frequency corresponding to energy adjusted to the bandgap, and d) injected electron or hole through CBC and VBC are contacts to conduction and valence bands, respectively, are absorbed and energy is dissipated in the device. The recycling can be either initiated by photon absorption or charge carrier injection and ends either:

- when the built-in field breaks the generated pair and separates the electron in conduction band from the hole in valence band so that the electrode linked to the conduction band (CBC) in n-doped region absorbs the electron and the electrode linked to the valence band (VBC) in p-doped region absorbs the hole, that is case (a) in Fig. 6. The net result is a separation of electron-hole pairs. The minority carrier currents are shown in Fig. 6 with a brown double-line arrow, solid for the electrons and dashed for the holes.
- or with production of a photon that exits the device, cases (b) and (c) in Fig. 6.

Also electron (or hole) injection from the solar cell electrode (into the device) initiates the "photon recycling" process, without requiring incoming photons. The injected electron contributes into the dark current but only when a photon induced by the "recycling" exits the cell as shown in Figure 6 (c). Otherwise the electrode absorbs the earlier injected electron as it is shown in Figure 6 (d).

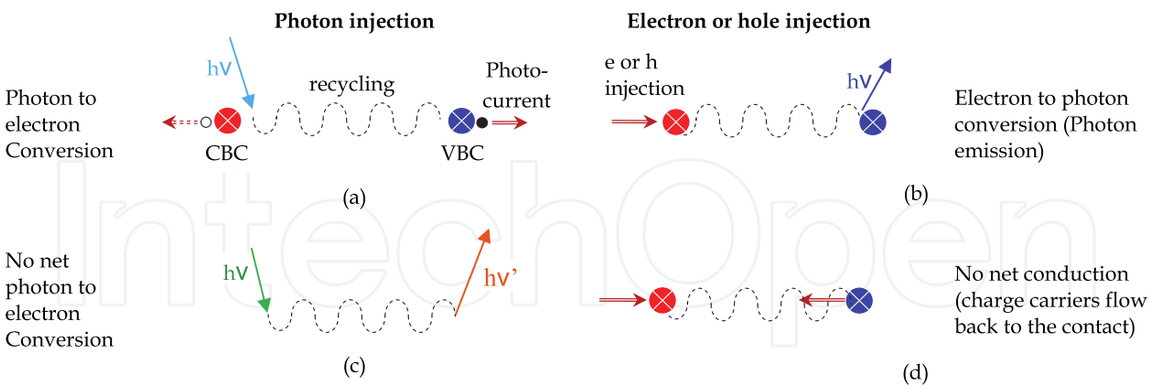

Fig. 6. Feynman-like diagrams for various electron-photon processes in a PV cell. Single and double arrows represent photon and electron, respectively. The periodic path represents the recycling processes of absorption/emission and generation/recombination of photons and electrons, which occurs while the particles propagate in the solid.

2.3.3 Shockley-Queisser limit

For evaluation of the photovoltaic conversion maximum efficiency, Shockley and Queisser have developed a thermodynamic approach based on the detailed balance principle

(Shockley & Queisser , 1961). They have considered the ideal case of solar cells made of perfect materials bestowed with radiative inter-band transitions only. Shockley and Queisser arrived at the paradigm that consisted in equalizing the photo-current and dark-current to the net flux of incoming and emitted photons (Shockley & Queisser , 1961). The most important idealization conditions they have considered are:

- non-radiative interband transitions are prohibited,
- the semiconductor structure is thick enough to ensure full absorption of incoming photons that are able to induce interband transitions in the absorber,
- carrier mobility is infinite so that the quasi-Fermi levels FC and FV exist, respectively, in the conduction band for electrons and in the valence band for holes, and
- contacts are ideal so that one of ohmic contacts absorbs **only electrons** from the conduction band and the other absorbs **only holes** from the valence band.

Dominance of radiative transitions in inter-band transitions maintains electron-hole pairs through "photon recycling". This is schematically illustrated in form of "Feynman-like diagrams" in Figure 6.

In their hallmark model, Shockley and Quiesser have used ideal semiconductor materials where *only radiative electron inter-band transitions are possible*, thereby enabling the development of the detailed balance principle. Fermi's Golden Rule application to electron transitions leads to the same matrix elements for direct and opposite electron transitions in solids so that each photon absorption induced electron transition has its radiative recombination counterpart. The balance of these processes depends on the occupation of the relevant electronic states. The detailed balance principle claims that the net of direct electron transitions between two energy levels equals to the net of opposite electron transitions if the sub-system of the levels is in thermodynamic equilibrium. Shockley and Queisser have shown that, because of intra-band relaxations, the "photon recycling" dynamics brings photon modes traveling long enough within the ideal semiconductor material into the thermodynamic equilibrium distribution of photon modes emitted by the "black body" material; so that the ideal PV cell emits "black body" modes, regardless of material and solar cell structure. Figure 6 shows that the net of photon fluxes emitted from and incoming into the solar cell equals to the net of dark- and photocurrents. One can easily estimate the photocurrent, the dark current, and the conversion efficiency of ideal solar cell. Figure 7 displays conversion efficiencies of *single-junction* based solar cells under normal illumination condition (1 sun) and under full solar light (theoretically possible) as a function of the absorber bandgap (Shockley & Queisser , 1961). The chart shows the Shockley-Quiesser limits for both illumination conditions.

The Shockley-Quiesser detailed balance theory estimates the lowest bound for all recombination processes throughout the device. This lowest bound defines the limit of attainable value of the dark current, which is the recombination rate integrated over the device volume confined within the electron diffusion length. This limit is important because it estimates the potential of the dark current reduction in devices by cleaning materials and improving the device structure.

2.3.4 Luque-Marti limit for quantum dot intermediate band solar cells

The foundation of Intermediary Band (IB) within semiconductor bandgap is very attractive for high efficiency solar cells. In principle, it can be applied for any semiconductor base material, but the benefit differs for one material to another. Formation of IB enables absorption of low energy photons on top of the conventional band to band absorption of

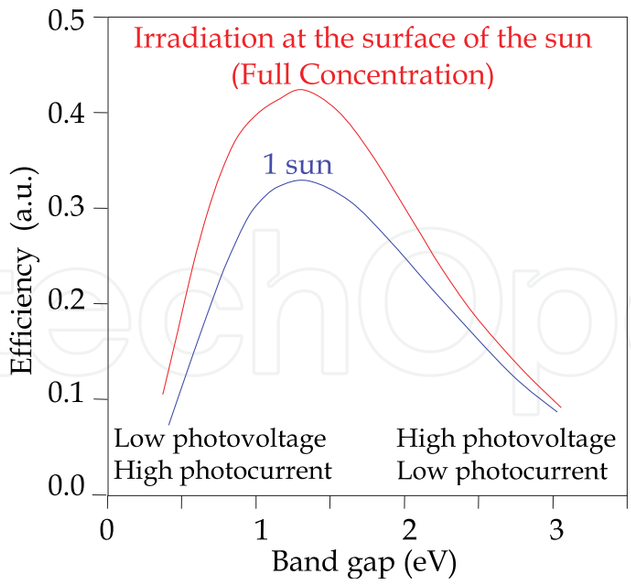

Fig. 7. Limiting efficiency of one-junction conventional solar cells.

photons with energy equal or higher than the bandgap. As shown in Fig. 5, low energy photons that are not converted by conventional silicon solar cells represent a major loss, which justifies the endeavor of modifying silicon to become an IB enabled material.

IB solar cells indeed promise very high conversion efficiency, higher than multi-junction solar cells. New solar cells can use IB states to enable absorption of low energy photons and promote more electronic transitions. This results in producing additional photocurrent and subsequently, a significant increase of solar cell efficiency. However, IB may also induce more recombination of electrons and holes in solar cells (Kechiantz et al., 2007; Kurtz et al., 2005). Because the Shockley-Queisser theory has not considered photogeneration and recombination processes through IB states, Luque and Marti adapted the Shockley-Queisser theory to model IB based solar cell throughput. Guyot-Sionnest et al., (1999) have evaluated the conversion efficiency of ideal IB solar cells in the framework of a new theory.

The IB can be composed by modification of a host semiconductor. A variety of routes can be employed, such as embedding quantum dots (QDs) in a host semiconductor (Marti et al., 1999). An idealized model for the electron energy band diagram in IB solar cell and the associated optoelectronic mechanisms is shown in Figure 8(a). Like in conventional solar cells, absorption of high energy photons brings electrons from the valence band (VB) to the conduction band (CB). Likewise, absorbed low energy photons move electrons from the VB into IB and from IB into the CB , either in synch or differed sequences, depending on the occupation of the states within the IB. The net result is a two-photon absorption with a displacement of an electron from VB to CB.

Luque and Marti have optimized IB energy levels within the bandgap of the base material to match solar spectrum. The matching leads to the utmost net VB-CB electron transitions. The red curve in Fig. 8 (b) displays Luque-Marti limit for conversion efficiency of IB solar cells; the indicated parameter is the higher among energy gaps from VB to IB and from IB to CB. These conversion efficiency curves have been calculated for ideal cells with the following ideal conditions:

- a quasi-Fermi level, F_I , exists for electrons in IB states, and

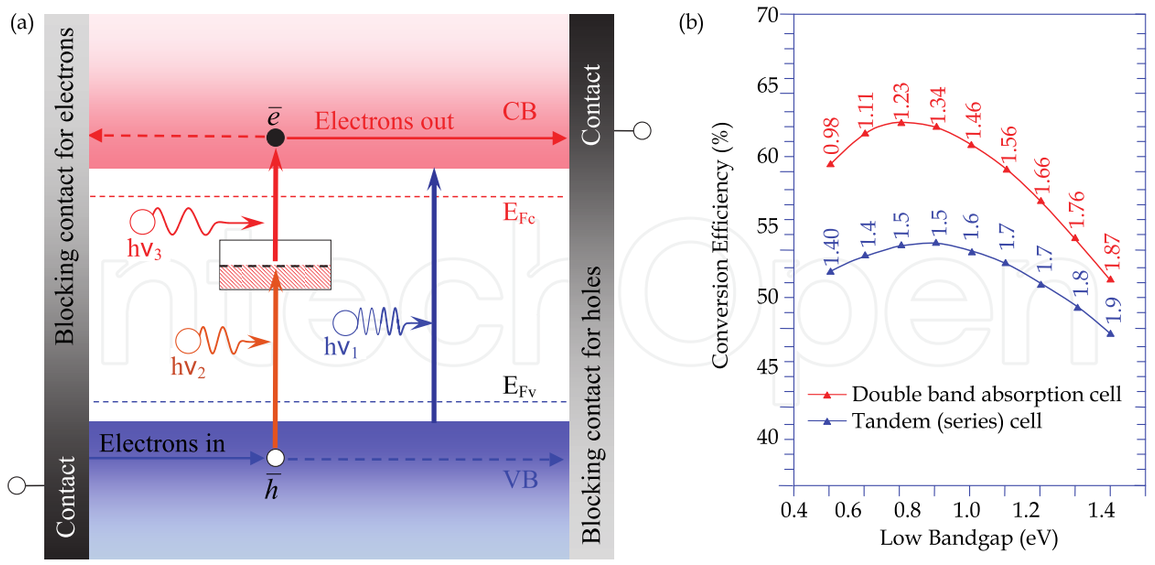

Fig. 8. (a) Energy band diagram of IB solar cell and (b) cell efficiency limits for various IB materials (modified chart in Ref. of Luque & Marti, 2010). Materials with the same bandgap used to make a tandem cell (a completely different cell design) would lead to much lower efficiency limit, as shown with the blue curve.

- no carrier can be extracted from IB into n- and p-doped regions other than by radiative interband transition to continuous bands either VB or CB.

Experiments have confirmed that missing either of the above requisites reduces the efficiency of IB solar cells (Alguno et al., 2006; Luque et al., 2004; Jolley et al., 2010). Also electron transitions through IB must have large matrix elements and solar cells must contain high concentration of IB states for maximizing the generation of additional photocurrent. The red curve in Figure 8(b) exhibits the maximum conversion efficiency for IB solar cells, which is 8 points larger than that for the ideal two-junction tandem solar cells (blue curve). This significant difference is essentially due to a difference in IB solar cell concepts compared to its multi-junction counterpart. While both concepts increment the high energy photon conversion by the low-energy photons in the solar spectrum for achieving higher conversion efficiency, the resulting *photovoltages* are dissimilar. The multi-junction solar cells exploit single-photon absorptions in an array of p-n-junctions connected in series. As the IB solar cells collect current from concurrent processes, the photovoltage can be approached by that of two cells with different bandgaps connected in parallel. In reality, the photovoltage precept is rather more complex. Besides, when an IB cell is shone with *concentrated sunlight, nonlinear effects* driven by the two low-energy photon absorption become significant, which essentially *increase* the generation of *additional photocurrent* in single p-n-junction solar cells (Sun et al., 2006).

2.4 High efficiency solar cells

2.4.1 Down- and up-conversion of solar photon energy

Figure 9 exhibits Si absorption coefficient spectrum and solar energy losses in conventional silicon solar cells. About 10% of incoming solar photons under AM1.5 condition has energy above $3.2eV$. These ultraviolet photons are absorbed in ultra-shallow region, about $10\ nm$

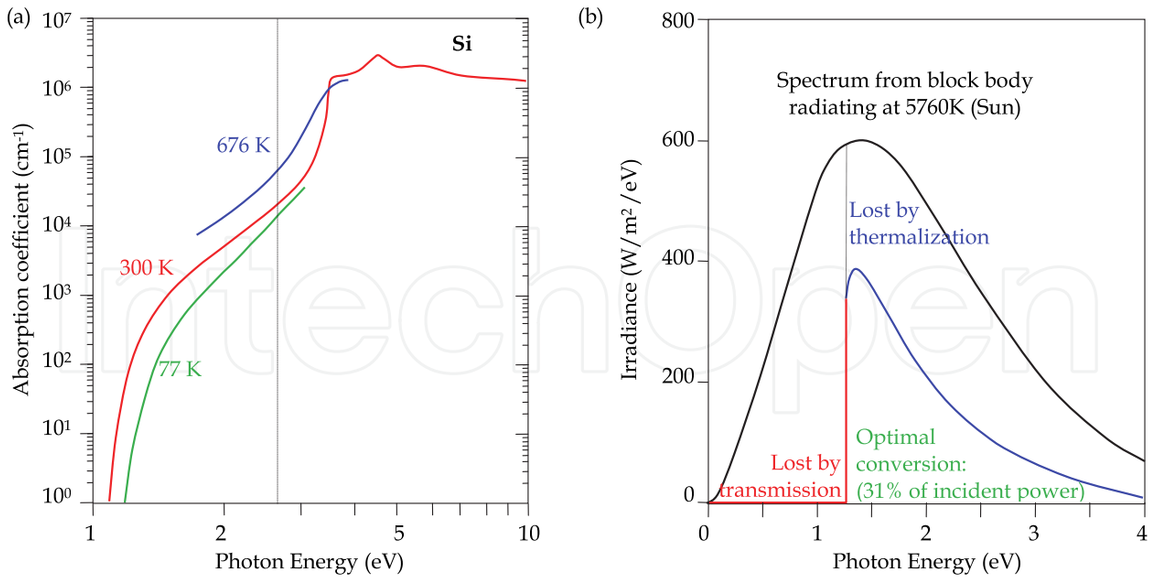

Fig. 9. (a) Absorption coefficient in Si and (b) spectral balance of main losses of solar energy in a one-junction solar cell.

thick in silicon, called the cell dead region because the recombination at the surface eradicates photo-generated carriers.

About 10% of incoming solar photons shown in Fig. 5 have energy above 2.5 eV ; which is in excess of the energy needed for generating two electron-hole pairs in conventional silicon solar cells (Green, 1998). However, these photons lose most of their energy (in excess of Eg) through intra-band thermalization, as shown in Fig. 9 (b). The *down-conversion* consists in directly splitting the incoming high energy photons into two lower-energy photons or for that matter converting primary optical phonons in low-energy photons. The *down-conversion* has two features, (i) utilization of the excess energy to better match the absorber bandgap leading to more electron hole pairs, and (ii) low energy photons have longer absorption depth and electron-hole pairs can be collected in other areas of the cell. Both features lead to generation of more photoelectrons away from the dead region (Baumgartner et al., 2010).

Also photons with energy lower than the bandgap, represented with small arrow (c.) in Fig. 8, can be used to generate additional photo-carriers in solar cells. Sequenced transitions of two of such photons may, indeed, result in a net ascension of electron to the conduction band. Under some conditions, the most probable path for the electronic system to return to its fundamental state is a radiative transition directly to the valence band. The net effect is the production of a photon of higher energy than the initial ones; this is called *up-conversion*. When up-converted, photon energy matches semiconductor bandgap and hence enables generation of additional photocurrent in solar cells. Noteworthy, the up-conversion is essentially non-linear quantum mechanical effect that gains from sunlight concentration.

2.4.2 Intermediate band for nanostructured silicon materials

Intermediate band (IB) solar cell concept exploits the up-conversion. It uses two low-energy photons for generation of additional photocurrent in solar cells (Luque & Marti, 1997). The detailed balance theory of ideal single p-n junction solar cells allows estimation of conversion efficiency limit of 31% using conventional single-photon absorption mode

(Shockley & Queisser , 1961) and 63% efficiency limit for operation in IB-mode (Luque & Marti, 1997). Such large gain in conversion efficiency will be discussed in more details below.

Like impurity states, QD confined states are easily transformed to fast recombination centers. However, there are experiments that show Type-II QDs made from indirect bandgap materials do not degrade electron–hole recombination lifetime (relative to that of host semiconductor without QDs). The reason stems in the spatial separation of carriers in such QDs. Photo-carriers have much longer lifetime in indirect bandgap materials used in commercial solar cells because phonons must absorb excess momentum, which delays electron–hole recombination. For historical and technical reasons silicon materials have gained incredible advances in material growth and processing. As a consequence, fabricated Si devices have low defect concentration that otherwise degrade carrier lifetime. For instance, electron–hole recombination lifetime can reach 100 μs in CZ Si wafers and epitaxial films and more than 10 ms in float zone silicon. Enhancing photon absorption of indirect band material by hosting specifically designed quantum dots (QDs) opens new opportunities for the foundation of intermediary band (IB) states.

Our choice lies far from standard approaches to PV cell design; we believe that the indirect bandgap silicon, which has poor absorption over the solar spectrum, has a lot of room for improvement through the set-up of an IB. Furthermore, single junction IB cell offers room for significant design optimization.

2.4.2.1 Two approaches to Intermediate Band solar cells

Both IB solar cell concept and the above mentioned requisites (listed in section 2.3.4) do not presume a specific location of IB states in the cell. There are at least two ways for incorporating materials featuring IB(s) in a PV device, which are (i) *within the depletion region* (Luque & Marti, 2010) and (ii) *outside the depletion region* (Sun et al., 2006) of a p-n junction solar cell. Figure 10 (b) displays the energy band diagram of IB solar cell that has type-II QDs imbedded outside the depletion region (Sun et al., 2006) in contrast to the pioneering scheme of IB solar cells, Fig. 10 (a), where QDs are sandwiched within the depletion region between p- and n-doped layers (Luque & Marti, 2010). Recent experiments with InAs QDs embedded in the built-in electric field of depletion layer sandwiched between n- and p-doped GaAs layers have demonstrated that photovoltage of such IB solar cells is lower than in the reference GaAs solar cell (Luque & Marti, 2010). It was proposed that the reason was the overwhelming thermal generation of carriers in InAs QDs. Perhaps InAs/GaAs is not

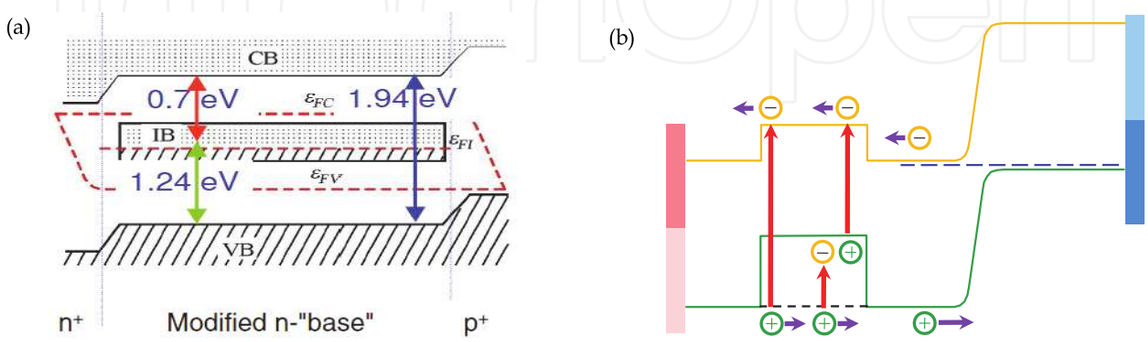

Fig. 10. Two strategies for IB formation in one-junction solar cell: (a) IB within the depletion region (Luque & Marti, 2010); and (b) IB outside the depletion region (Sun et al., 2006).

the best material system for making IB solar cells (Sun et al., 2006). It has then become clear that QDs within the depletion region enhance the dark current.

The recently proposed IB scheme proposed by Sun et al. (2006), see Figure 10 (b), where type-II QDs are placed outside the depletion zone of the cell p-n junction offers the advantage that such QD configuration does not generate additional leakage current. The leading reason is the remoteness of QDs from built-in electric field. This key property isolates confined holes from that field. While holes cannot escape from QDs they still reach the p layer without assistance (for instance from photons, etc….). In the meantime p-n junction separates all mobile photo-carriers generated within a distance less than the carrier diffusion length from the junction and with states either in the VB or in the CB. Such separation includes also photo-carriers transferred trough QD confined states to the continuous bands.

Another important advantage of type-II QDs is the energy band alignment, which results in a potential barrier for majority carriers and a potential well for minority carriers. Such an alignment is shown in Fig. 10 (b) along with carrier transitions and flows. The potential barrier separate carriers photo-generated within the QDs, and hence suppress electron-hole recombination through QDs (Sun et al., 2006). Charge segregation by the QD built-in barrier is an essential feature for irradicating electron-hole recombination in QDs. Energy conversion in IB solar cells strongly depends on the separation of electron and hole quasi-Fermi levels (Kurtz et al., 2005), while recombination through QDs may result in lining-up those quasi-Fermi levels. Hence, it has been argued that QDs confined states can easily turn into fast recombination centers. Likewise, impurities incorporated in GaInNAs solar cells exhibit such conversion into recombination centers (Zibik et al, 2009), whereby the quasi-Fermi level is affixed to the impurity energy level and subsequently the carrier recombination is enhanced. As a result, the photovoltage is degraded to a level lower than expected for GaInNAs solar cells.

Figure 11 shows that sunlight concentration leads to the rise of additional photo-induced potential barrier around type-II QDs in valence band for the new "off-field QDs" strategy (Sun et al., 2006) thereby constituting a new type of IB solar cells. Additionally, such photo-induced barrier suppresses recombination activity of QDs, which results in a more effective two-photon absorption in QDs. Above some value of sunlight concentration the photoelectron generation dominates the recombination in QDs so that the photocurrent generation and the conversion efficiency of such IB solar cell become higher than in the reference solar cell become higher than of a reference cell made of same material and a conventional single p-n junction (Luque et al., 2004).

2.4.2.2 Design of IB solar cell

As the characteristic dimension of solar cell active zones is falling in the nanometer scale, quantum phenomena like the electronic confinement in nanofeatures come to play. These must be adequately used for developing modern electronic and optoelectronic devices and more so the vital third generation solar cells. A detailed understanding of fundamental quantum processes taking place in charge carriers and phonon systems generated within such electronic nanostructures is required. Moreover, those quantum processes must be consolidate with other effects that might otherwise hinder the sought high efficiency devices.

Quantum properties of low-dimensional structured materials are very attractive for designing unique solar cells (Aroutiounian et al., 2001; Nozik, 2002; Luque & Hegedus, 2003;

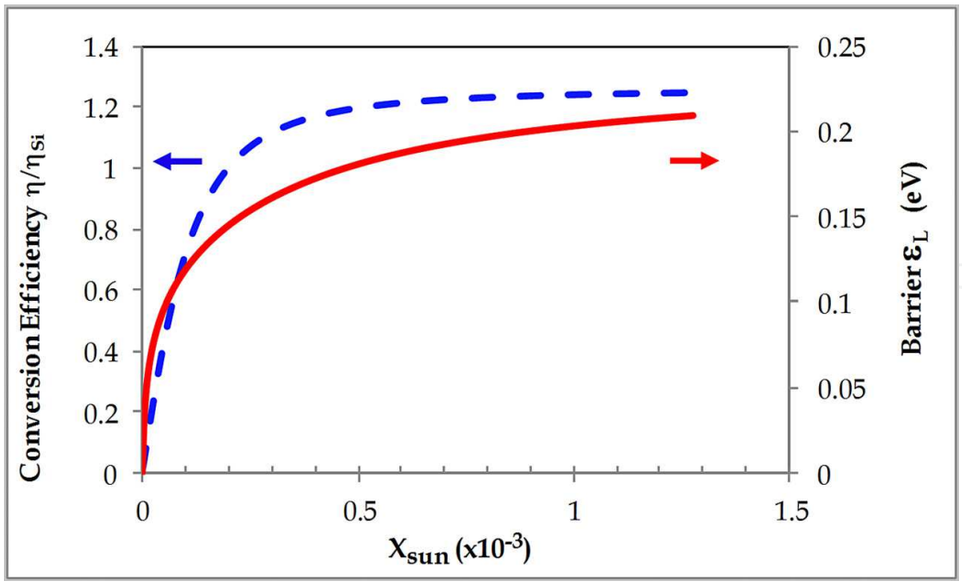

Fig. 11. Irradiation-induced barrier ε_L (dashed line) and conversion efficiency η/η_{Si} (solid line) as a function of sunlight concentration X_{sun}, where η is the conversion efficiency of Ge QD based solar cell and η_{Si} is the efficiency of the reference solar cell (Sun et al., 2006). The reference cell is a Si PN homojunction. The Ge QD induce an IB in the host material outside a similar PN junction.

Tsakalakos, 2008), in particular, IB solar cells with QDs (Marti et al., 2000) QDs imbedded in conventional solar cells introduce resonant energy levels that can be configured to compose a narrow band in the host material band gap (Luque & Marti, 2010). Although silicon is an excellent semiconductor for microelectronics, its indirect bandgap made it inefficient for light absorption, for this matter compare for instance Si absorption coefficient to that of GaAs in Fig. 12. Traditional silicon solar cell design uses at least 150 μm thick wafers to allow capturing enough sunlight. The used substrate is 15 to 20 times thicker than its III-V counter-part. Because of the low absorption and the use of massive material, silicon is in fact not ideal for photovoltaics, and since this expensive material has taken the largest segment in industrial photovoltaic, solar electricity remained a very expensive commodity. The poor absorption makes thick crystalline silicon based PV not apt for further development and cost reduction. However, nanotechnology is being explored to remedy to the silicon fundamental issue of low light absorption. The wide-range of processing knowledge attained during the formidable development of microelectronics, for which silicon still constitutes the base material, can be indeed utilized to compensate the drawbacks of poor light absorption. Also PV silicon suffers from a second problem that is related to the absorption band edge. Wide bandgap semiconductors use more efficiently energy of incident photons as they enable the photocurrent to generate higher photovoltage, whereas the narrower bandgap materials lead to more loss via thermalization of the energy in excess of the bandgap. Silicon bandgap width is considered in the midrange of a host of semiconductors used in photovoltaics. Nevertheless, the loss of high energy excess by thermalization remains considerable in silicon and a solution must be provided.

The large amount of loss practically obstructs one from obtaining high efficiency silicon photovoltaic devices. Industry has been struggling, indeed, for improving silicon solar cell

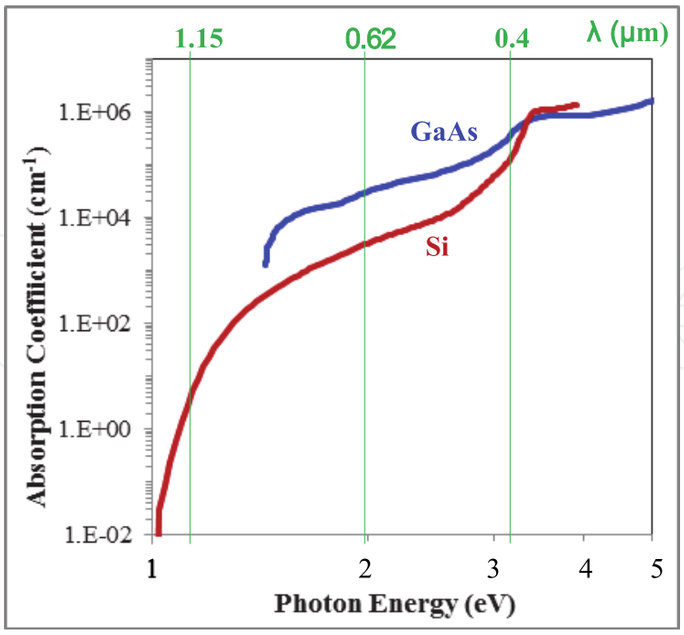

Fig. 12. Direct bandgap (GaAs) versus indirect bandgap material (Si) absorption coefficient.

efficiency at a fraction of percent leaps, while they are getting closer to the theoretical limit. After decades of R&D the fabrication of silicon homojunction solar cells reached its best and has proven to be extremely robust. However, the quantitative assessment of the effect of the bandgap width given in Figs. 4, 5, and 9 shows the shortcomings of the use of silicon in photovoltaics. The main hurdles for PV silicon are the bandgap value, the indirect type and consequently the low light absorption. This explains the efficiency limits over which the PV industry is confronted. Fabrication processes can only be refined for lowering cost and increasing their yield, without adding energy conversion efficiency points that the business is craving of.

However, indirect band gap materials like Ge type-II QD/Si are attractive for IB based solar cells (Sun et al., 2006). This provides an opportunity to overcome the efficiency limitation the current industry is suffering from. Noteworthy is the very slow electron-hole recombination property of IB enabled Si material, which can be exploited for achieving higher efficiency. The large band discontinuities and the real-space indirect fundamental bandgap at the interface in type II Ge QDs embedded in Si are favorable, indeed, for the reduction of carrier recombination. For instance, electron inter-band recombination lifetime is extended to 1 μs in type II Ge QDs in Si (Fukatsu, 1997). Also up to 0.3 eV conduction band offset is possible in this system, which depends on the strain at the interface and the composition of Si spacers (Schaffler, 1997), hence it can be tuned by controlling the strain. Simple tuning can be done by isoelectronic impurities such as Sn, C. The, small C atoms compensate the strain induced by Ge (Schmidt & Eberl, 2000). But the most favorable feature offered by Ge QD, although Ge is an indirect band gap material, is the large cross-sections for photon absorption (Boucaud et al., 1999). Of equal importance is the compatibility of Ge material with Si based technologies, leading to a lower cost integration of Ge in production processes than with other materials.

Luque-Marti concept of IB solar cells does not put limits in the choice of IB material systems and structure. Transition-metal impurities in substitutional positions in III-V compounds

have been under consideration. Narrow energy band predicted in the Brillouin zone of Ga_4As_3Ti compound is shown in Fig. 13, (Wahnon & Tablero , 2002) where an IB.

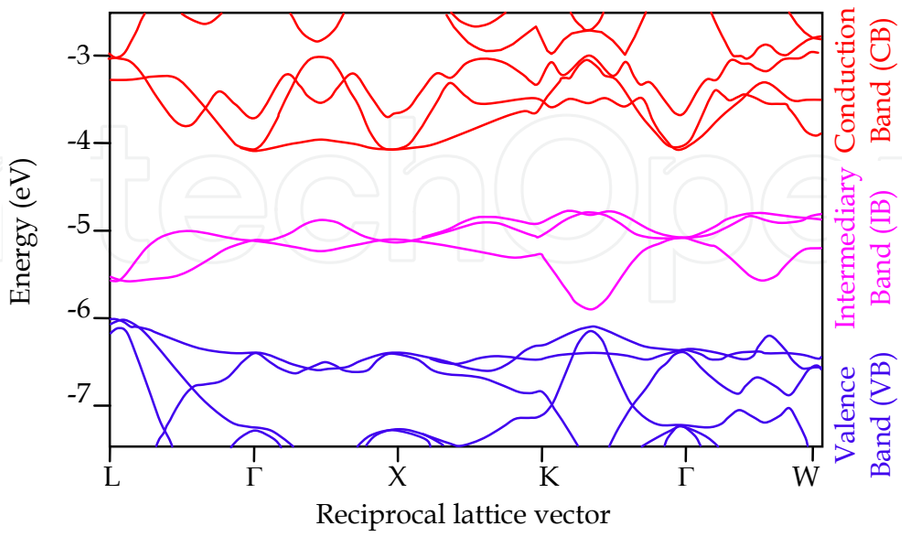

Fig. 13. Transition metal (Ti) induced IB in energy band of III–V compounds, Ga_4As_3Ti (Wahnon & Tablero , 2002).

Layers of alloys with large lattice parameter mismatch is another group suitable for IB (Yu et al.,2003). A relatively small fraction of substitute atoms like nitrogen in III-V compounds and oxygen in II-VI compounds, which are more electronegative than the isovalent host atoms, are used to generate specific features in the electronic structure of such alloys. Figure 14 (a) displays energy band structure of $Zn_{0.88}Mn_{0.12}Te$ with oxygen in substitutional sites, for which one can see the IB right in the middle of the bandgap.
As grown porous silicon (PS) and sensitized PS are the next material systems with unique IB potential for photovoltaic that are proposed by the author and will be studied in the second part of this chapter.

3. Intermediary band enabled silicon for nanostructured PV devices

3.1 Introduction

The currently sought cost reduction of silicon solar cells compels for searching new paradigms for designing solar cells capable of outperforming the widely used silicon solar cells. Hence, modifiers that can make more efficient optoelectronic processes in silicon are desired, while the cost of these substitutes must remain low. Thin film PS is one of such alternatives with a wide range of quasi-classical and quantum properties that can be utilized beneficially for developing the sought new photovoltaic paradigms.

3.2 Quantum properties of nanostructured porous silicon

Electrochemically generated PS constitute a class of complex materials featuring a wide range of possible functionalization. PS chemical composition and surface states vary in a myriad of ways due to fluctuations of etching parameters and exposure of the open surface to chemicals. These appear manageable though. For instance, the size of pores and inner

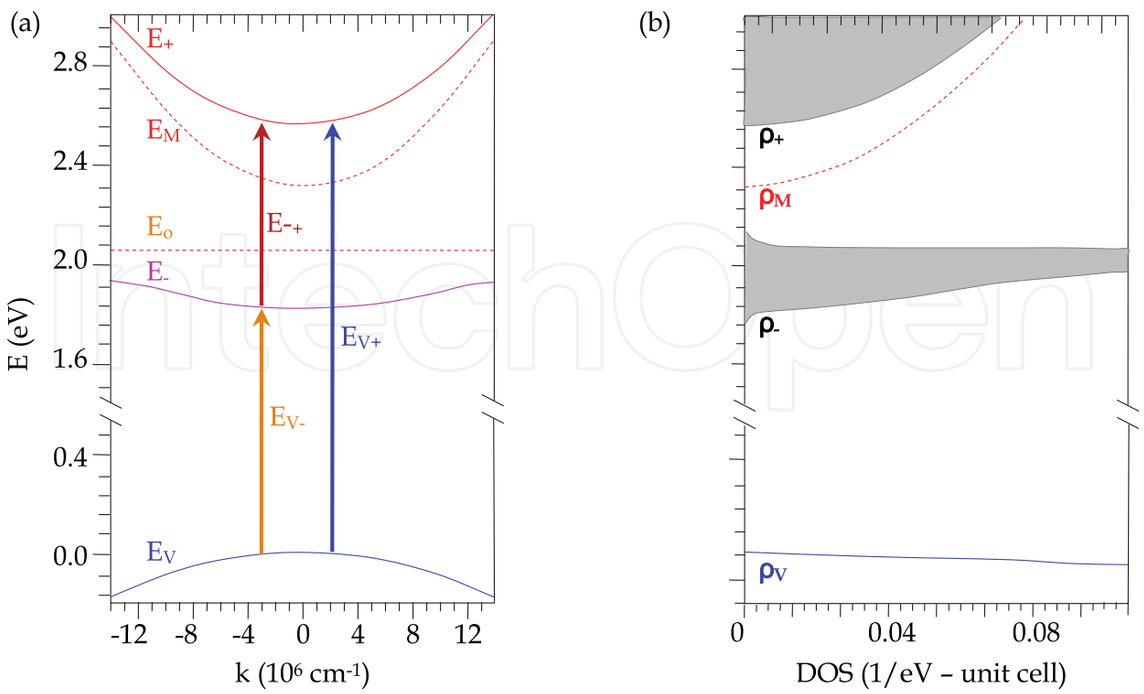

Fig. 14. (a) Band structure of $Zn_{0.88}Mn_{0.12}O_xTe_{1-x}$ with x=0.01 oxygen, exhibiting an IB and (b) the corresponding density of states (Yu et al., 2003).

walls can be deliberately designed to be from a few nm to hundreds; the wall structures can vary from nano- to micro-size and they can contain silicon crystallites and silicon amorphous phases. Porous silicon showed strained silicon phase, that was interpreted based on Raman shift as embedded in oxide (Karoui, 2010). Radiative recombination showed a surface composition that is sensitive to the ambient (Karoui & Zhang, 2010). Potentially, pores may be filled with nanoparticles, or clusters of impurities of other materials attached with physical or chemical bonds to the inner wall surface. Such complexity also provides PS with some useful properties. For instance, QDs can enable PS with electron energy IB. QD sensitized PS is a unique new material system studied by the author for making new solar cells (Karoui & Kechiantz, 2011). For the quantum effects come to play, the electron wavelength must be comparable to the feature size of the considered system, e.g. in QD arrays. Interference of interacting electrons confined in so small volume of a QD may result in quantum effects like Coulomb blockade of electron current through that volume and conductance oscillation. These have been observed in devices like the single electron transistor (SET) (Aleiner et al., 2002). Coulomb blockade enables very strong control of electron transport through SET channel so that the gate switches from insulating state to conducting with one electron charge accuracy (Ai et al., 2010).

Likewise, modified PS that has pore size in the range of several deca-nanometers can behave as a quantum system if the characteristic size of the modifier (here QDs) is comparable with the electron wavelength in that material. Electron energy bands in solids arise from initially discrete energy levels of a very large number of atoms. Each of these N atoms contributes an electronic state so that the initial *s* and *p* atomic levels shown in Fig. 15 are twice N-fold degenerate, considering the two spin states. Reduction of the distance between initially separated atoms brings the orbitals closer, which enables electron

tunneling between neighbor atoms. Furthermore, reduction of inter-atomic distance increases electron interaction in neighboring orbitals, and makes overlapping of electron orbitals possible. In the meantime, interference of interacting electrons enables coherence of their quantum states. This liberates electrons, initially confined around isolated atoms; as a result initial atomic levels are no longer degenerated and are transformed into continuous bands. As the interatomic distances are brought to an optimal value, electron correlation gets stronger and the bands get wider. The well-known diagram given in Fig. 15 illustrates the transformation of energy levels of an atomic assembly into energy bands of the henceforth formed solid. At the atomic spacing R_0 the energy of the assembly is minimal and thus R_0 is the equilibrium interatomic distance at which the assembly becomes stable.

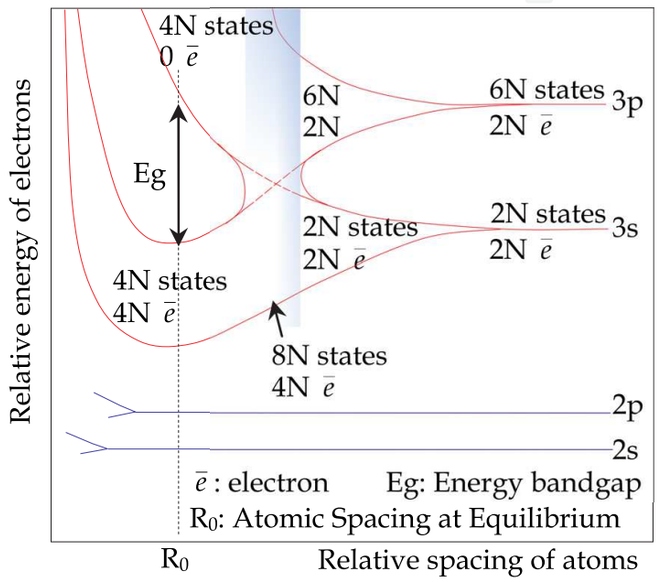

Fig. 15. Merging atomic levels into energy bands in solids.

3.3 Functionalization of porous silicon and size effects

The discrete energy spectrum of Ge QDs buried in crystalline Si modifies the host crystal physical properties. Modification of a host semiconductor with QDs produces material with electronic and optical properties that essentially depend on the size, strain and composition of QDs. However, many other factors like composition of a cap deposited onto a QD layer, separation distance between QDs, strain driven material inter-diffusion at the interface, etc., contribute in the modification of the host material electronic structure. While small QDs are more sensitive to material inter-diffusion, quality interfaces are required for effective charge carrier confinement in small (less than 10 nm) Ge QDs at room temperature (Derivaz et al., 2002). Nanofabricated Ge QDs and the underlying physics have become subjects of thorough investigation for clarifying many new features as these material systems offer humongous potential for using them in making photodetectors, lasers, quantum computers, etc. (Halsall et al., 2004; Meyer et al., 1999). Some of those features have been briefly discussed below. Noteworthy, the behavior of Ge QDs buried in Si system has shown the great potential for building an IB enabled material by embedding Ge QDs in the PS material pores and to control the characteristics of the generated IB.

The understanding of the role of discrete levels in quantum dots and associated electron standing wave-functions, the bunching of energy discrete levels into bands, the origin of splitting of these levels in relation to the coherency of the electron wave tunneling, etc… are crucial for the design of the IB enabled materials. The coherent tunnelling of quasi-confined Bloch wave functions in a finite array of quantum dots (for instance Ge QD attached to inner surfaces of grooves and cavities in porous silicon in the herein discussed case) will emerge as a main mode for charge transfer between QDs and the host material. Carrier tunnelling through critical spacing and its quantum mechanical origin and the coherency of tunnelling waves will be discussed based on calculated electron probability. The quantum levels for QD assemblies and effect of inter-particle transparency, akin to the bunching of atomic levels into energy bands discussed above will be appear, they will depend on the coupling between QDs within the QD array.

3.3.1 Strain induced separation of confined charges

It was reported (Fukatsu, 1997) that diffusion of Ge and the onset of the strain in the Si cap layer may cause spatial separation of confined carriers, i.e., separated holes and electrons. Large mismatch in lattice constants and difference in thermal expansion coefficients enables Si substrate to strain Ge QDs and favors self-assembly of Ge type-II QDs (Lee & Wang , 1994). Most of the band offset occurs in the valence band so that such QDs confine only holes. Square-based pyramidal shape (side ≈100 nm at the base) Ge QDs exhibited intraband absorption at around 300 meV (Boucaud et al., 1999), the authors attributed it to bound-to-continuum transitions in the valence band. The density of these QDs was about $2\times10^{9}\,cm^{-2}$ and they exhibited an in-plane absorption cross-section of about $2\times10^{-13}\,cm^{2}$. However, filling the ground state with electrons saturates intraband absorption in those QDs. The use of a virtual substrate, which is a thick buffer layer on graded SiGe, results in a different in-plane lattice constant of the add-on layer due to relaxation. Virtual substrates change the strain configuration in Ge QDs (Fromherz et al., 1994). The $Ge_{1-x}Si_x$ / Si interface layer may become partly strain-free alloy. The new configuration can favor also electron confinement in SiGe buffer layer near Ge QDs so that the structure spatially separates electrons and holes in QDs (Meyer et al., 1999). Inter-subband absorption experiments confirmed such confinement of electron-hole pairs in Ge QDs (Lee & Wang , 1994).

It was reported that free-standing hut clusters of pure Ge are formed at 500°C (Denker et al., 2003) by self-assembling Ge on Si (001) substrate. Photoluminescence characteristic line of these huts is more than 120 meV below the band gap of unstrained bulk Ge, which suggests that a cap Si layer compressively strains huts of pure Ge. The results indicate that the photoluminescence originates by indirect transitions of electrons confined in Si substrate (in the QD vicinity) to holes confined in the strained Ge islands. An activation energy of 40 *meV* ensures that these electrons remain confined around Ge type-II QDs, which is very close to the energy of electron-hole bounding in a neutral exciton (Denker et al., 2003).

3.3.2 Control of QD shape and their density by ultrathin oxide layer

Ultrathin dielectric layer on the inner walls of PS enables the control of QD density. It was reported that 1.2 nm thick SiO_2 covering Si substrate allows production of Ge QDs at a density of 2 to $5\times10^{11}\,cm^{-2}$ (Derivaz et al., 2002). These dots are hemispherical with 10 nm average size. Based on the RHEED pattern the authors reported that the crystallographic orientations for deposited Ge QDs and the silicon substrate were the same. This points out to the local transfer of the substrate crystallographic order to the add-on material layer. The

transfer can occur through (i) small Si inclusions in the SiO_2 layer or (ii) the local re-order of the oxide layer (largely dependent on the interface stress relief mode). The spatial extent of these processes dictate the mode of self-assembling and the periodicity of the QD array.

3.3.3 Interface QD and host semiconductor

3.3.3.1 Inter-diffusion of Si and Ge at the QD/host material interface

Various techniques are used to fabricate small Ge QDs (smaller than 10 nm) on Si substrates. The most popular is the self-assembled QDs (Konle et al., 2003). Usually capping self-assembled Ge QDs with thin Si or oxide layer follows the formation of quantum dot arrays (Meyer et al., 1999). However, surface segregation and elastic strain relaxation drive QDs above the onset of plasticity to change shape and become flatter. Diffusion of Ge in silicon increases the lateral size of QDs and reduces their height, which may occur along with possible volume loss during the capping. Indeed, the composition of QDs may change during the capping process and even dissolve completely in the surrounding material. More importantly, the capping can induce a strong strain resulting in modification of the QD energy band structure within the QD and in its vicinity. Scanning tunneling spectroscopy study of silicon cap layer showed that deformation of the cap by Ge QDs reduces the band gap of the strained parts of Si cap at the surface (Meyer et al., 1999). The understanding of such reduction is connected to coupling dimer bonds, i.e., Si atoms in the cap and the Ge in the QDs, to stretch in the presence of surface strain. Such stretch reduces overlapping of p-orbitals in the dimers and hence bonding and antibonding splitting of Si p-states may occur. The strain distribution around nanoparticles enables diffusion of Si away from the strained surface regions on top of the Ge nanoparticles. Meanwhile, Ge diffuses towards regions with higher tensile strain, which is one (or the main) driving force for self-assembling of Ge QDs (Tersoff et al., 1996).
Photoluminescence from Ge QDs on Si substrate displays about the same recombination spectral line, which spreads over 0.75–0.9 *eV* energy range, akin of the high Ge content $Si_{1-x}Ge_x$ QDs and quantum wells on silicon (Miyazaki & Fukatsu, 1999). The broadness of the line indicates significant inter-diffusion between Si and Ge QDs because small particles are very sensitive to the strain. Such inference is also consistent with recently reported theoretical and experimental results of Seok & Kim (2001). The effect of material diffusion must be taken into account in case Ge QD sensitization of PS.

3.3.3.2 Interface transparency

Even in the case of best silicon wafer cleaning via oxide removal, a few silicon oxide monolayers and some amount of chemically or physically adsorbed impurity atoms may still remain. The problem is even more acute for cleaning pore walls in PS (Arenas et al., 2008; Hao et al., 1994). When functionalizing PS with Ge, the remaining oxygen at the surface reacts with Ge during deposition of Ge into the pores of PS. This may result in the encapsulation of Ge QDs incrusted onto the PS walls within a few monolayers of mixture of GeO_2 and SiO_2. Such a layer around a QD constitute an oxide shell (Prabhakaran & Ogino, 1995) that physically separates the dots from the pore wall or other dots. The layer quality determines the transparency of QD-Si or QD-QD interfaces to electrons clinging onto inner walls of pores.

3.3.3.3 Germanium quantum dot-oxide interface

3.3.3.3.1 Decomposition of GeO_2

Electron transport trough Ge QDs incrusted in PS depends on composition of the interface oxide layer. Thus it is essential to precisely know the composition and other properties of

the oxide shell. While SiO_2 and GeO_2 have similar electronic structure, their band gaps are different, $9.0eV$ and $6.1eV$, respectively (Lin et al., 2010). Moreover, unlike SiO_2, GeO_2 lattice poorly matches with Ge lattice, is less stable than SiO_2 on Si, and is soluble in warm water (Prabhakaran & Ogino, 1995; Hovis et al., 1999). Decomposition of isolated GeO_2 into GeO does not take place below 700°C, however, GeO_2 covering Ge dot core has tendency to loose O and transforms to GeO interfacial layer even below 500°C (Prabhakaran et al., 2000). Any thermal processing deteriorates GeO layers. It desorbs with about $2eV$ activation energy into volatile GeO (Wang et al., 2010). This chemical behavior ultimately ends thinning the oxide shell. Ultimately, the thinning stabilizes at a certain thermodynamic equilibrium governed by desorption wells of O atoms and GeO complex out of the GeO_2 layer.

3.3.3.3.2 Dangling bonds at Ge/GeO_2 interface

Tracers ^{73}Ge and ^{18}O isotopes have revealed that interfacial reaction of GeO_2 with Ge generates oxygen vacancies and makes Ge/GeO_2 interfacial region oxygen deficient (Wang et al., 2011). Desorption of GeO occurs due to reaction of GeO_2 with the oxygen vacancies at the GeO_2 surface after diffusion of these vacancies through GeO_2 layer from Ge/GeO_2 interface to GeO_2 surface. Such diffusion is accompanied with the generation of a huge amount of interface states and defects (Kita et al., 2008). Distribution of generated dangling bonds increases from the middle of the bandgap towards conduction and valence band edges like the U-shape distribution of states at Si/SiO_2 interface. However, energy levels of Ge dangling bonds at Ge/GeO_2 interface are below the Ge valence-band maximum E_v, which makes them always negatively charged (Weber et al., 2007). The dangling bonds are acceptor-like and build-up a negative fixed charge at the interface (Afanas'ev et al., 2005). Such negative fixed charge repels electrons from interface. The repulsion is so strong that it prevents layer inversion (Dimoulas et al., 2006).
Both fixed charge and dangling bonds significantly degrade electron transport across the interface Ge QD-Si and between Ge QD-QD clinging onto inner walls of pores in PS.

3.3.3.3.3 Ge/GeO_2 interface passivation Oxygen instead of Hydrogen

The specific feature of Ge/GeO_2 structures is that its straightforward passivation with hydrogen is ineffective because interstitial hydrogen atoms act only as acceptors near Ge/GeO_2 interface (Weber et al., 2007). Repulsion of negatively charged hydrogen from negatively charged interface defects prevents hydrogen passivation of the dangling bonds. As a result, annealing in hydrogen leaves a high density of interface states in Ge/GeO_2 structure though it removes dangling bonds associated with Ge crystal surface atoms (Dimoulas et al., 2006).
It is interesting that high-pressure oxidation at 550°C may stabilize Ge/GeO_2 interface, suppress GeO desorption, and reduce to $2\times10^{11}eV^{-1}cm^{-2}$ the interface density of states (DOS) in the middle of the bandgap (Lee et al., 2009; Matsubara et al., 2008). This is a good example that solves numerous problems like suppression of GeO desorption but passivation of dangling bonds at Ge/GeO2 interface still persists. That is a problem that remains to be solved for obtaining to obtain a working for Ge QD IB PS structures. The problem needs to be solved by further improvement of fabrication technology.

3.3.4 Quantum mechanics model of QD incrusted in porous silicon pores

Identical QDs clinging onto cylindrical pore walls in an ideal PS can be modeled, in a first approximation, as a periodic necklace-like circular chain of QDs, see Fig. 16. Let r_1 be the radius of the pore and r_2 the inner radius of the chain so that the thickness of the chain is

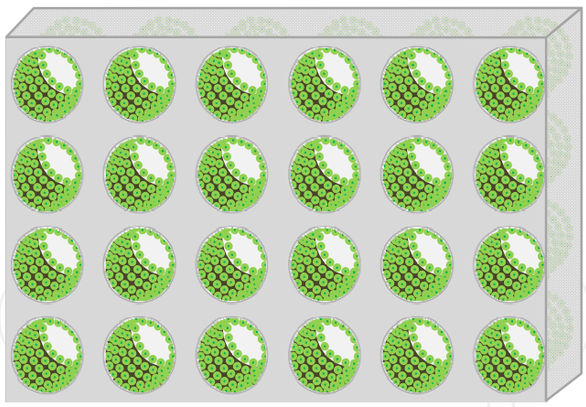

Fig. 16. QD rings inside porous material; in this work SiGe QDs in PS.

$(r_1 - r_2)$. The sketch in Fig. 17 illustrates such model, where the chain and the pore geometry are with perfect surface of inner Si walls.
One must take into account that few monolayer silicon dioxide layers always cover Si surfaces, even in clean silicon samples. Thus , aside from PS surface composition, Si QDs end-up being covered with an oxide shell. This natural oxidation ensures that the PS nanostructure is always covered by an oxide layer as shown in blue in Fig. 17(a). Furthermore, TEM imaging showed that oxide shell in PS separates the Si dots from the Si pore wall and from other dots.

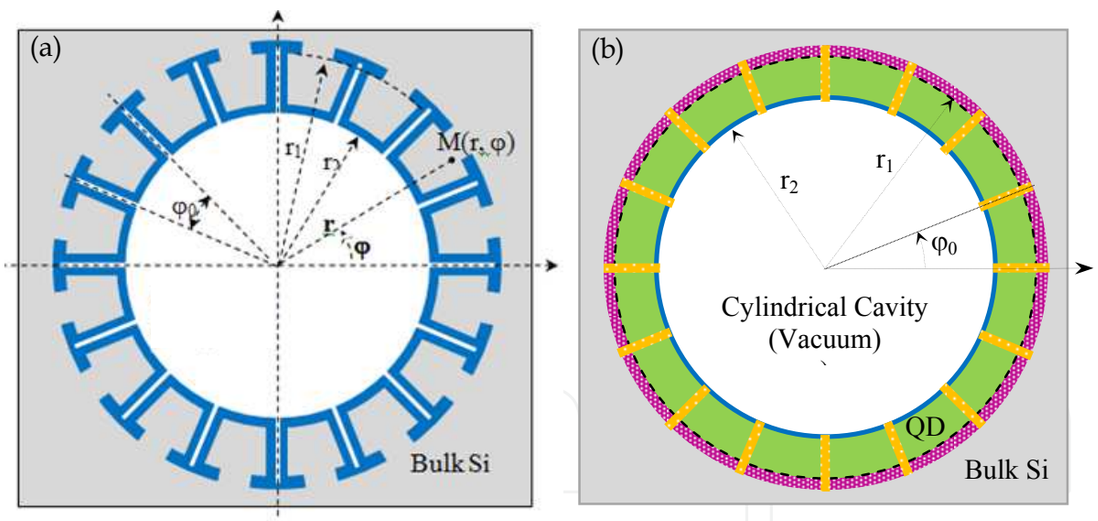

Fig. 17. Model of regular necklace-like circular chains of identical QDs clinging onto cylindrical pore walls in PS, Cross section showing one pore of the PS material and a set of Ge nanodots. The pink lines represent the transparency QD/Host material interfaces to electrons, while the yellow ones represent the transparency of QD/QD separation gaps.

3.3.4.1 Analytical model of QD incrusted in porous silicon pores

We have used polar coordinates (φ, r). QDs are $\varphi_0 r_1$ wide and the chain consists of n_0 QDs so that $\varphi_0 = 2\pi / n_0$.
Since QDs are "artificial atoms", they are expected to have similar energy band formation mechanism for all electronic states confined in an ensemble of closely packed QDs. However,

unlike infinite solids, a small number of QDs can be closely packed within a single pore in PS. Again, interaction and interference of quasi-confined electron waves results in coherence of electron states within such small chain of QDs, which behaves as an "artificial molecule".
Pore walls separate these artificial molecules from each other in PS, leading to a periodic array with symmetry specific to each direction. An artificial crystal is schematically shown in Fig. 17. Such functionalization scheme of PS is new, and has never been studied yet neither experimentally nor theoretically. The work is intended for photovoltaic applications, and will be published elsewhere.

3.3.4.2 Electron and hole wave functions

The simplified model assumes the effective mass approximation and null electron potential in QDs so that $V(r,\varphi)=0$ for $r_2 < r < r_1$. Schrödinger Equation (SE) in cylindrical coordinates, which reflects the symmetry of the physical model, for the electron and hole wave functions in such chain of QDs embedded in the PS can be written as follows:

$$-\frac{\hbar^2}{2m^*}\left[\frac{1}{r}\frac{\partial}{\partial r}\left(r\frac{\partial}{\partial r}\right)+\frac{1}{r^2}\frac{\partial^2}{\partial\varphi^2}+\frac{\partial^2}{\partial z^2}\right]\Psi(r,\varphi,z)=E\,\Psi(r,\varphi,z) \tag{1}$$

where:
- E and m^* are the electron (hole) energy and effective mass;
- $\Psi(r,\varphi,z)$ is the electron (hole) wave function;

r, φ and z are the radial, angular and axial components of cylindrical coordinates so that $r>0$ and $0<\varphi<2\pi$. Solution for equation (1) allows separation of variables, which reduces that equation to a set of ordinary differential equations for angular $\Phi(\varphi)$, radial $R(r)$, and axial components of the wave functions. The entire wavefunction can be written as:

$$\begin{aligned}\Psi(r,\varphi,z)&=C_{mk}\left[\exp(i\varphi m)+a\times\exp(-i\varphi m)\right]\\&\left[Y_m(kr+b)J_m(kr_2)-J_m(kr+b)Y_m(kr_2)\right]\sin(k_z z)\end{aligned} \tag{2}$$

where:
- m is the angular momentum quantum number;
- k is the radial momentum wave number; it relates to the electron energy E as $k^2=2m^*E/\hbar^2$, $J_m(kr)$, and $Ym\ (kr)$ are the first and second kind Bessel functions of order m,
- k_z is the axial momentum wave number,
- a and b are the integration constants, and
- C_{mk} is the integration constant that represents the amplitude of the wave function in the chain of QDs with respect to that in Si walls of PS.

The boundary condition for electron and hole wave functions is $\Psi(r_2,\varphi,z)=0$ at the inner surface of the chain inside the pore (QD-vacuum), where $r=r_2$. Such condition reduces the electron and hole wave functions within the chain of QDs, $r_2 < r < r_1$, to:

$$\begin{aligned}\Psi(r,\varphi,z)&=C_{mk}\left[\exp(i\varphi m)+a\times\exp(-i\varphi m)\right]\\&\left[Y_m(kr)J_m(kr_2)-J_m(kr)Y_m(kr_2)\right]\sin(k_z z)\end{aligned} \tag{3}$$

The energy band offset at Ge/Si interface is mainly in the valence band. This results in Ge QDs type-II energy band alignment in Si, which ensures that electron and hole wave functions meet different boundary conditions at the Ge/Si interface.

3.3.4.3 Boundary conditions and secular equation

3.3.4.3.1 For holes

We have already illustrated (in section 3, which is about quantum features of nanostructured porous materials) that the close proximity of atoms and the discrete relationship of their energy levels result in the band formations in solids. The same occurs with "artificial molecules" by the Ge QDs ring located inside a pore of PS matrix. If QDs are close enough, the discrete energy levels may form energy bands in the chain of QDs. Transparency of the interface (oxide) layer between QDs controls the phase relationship and induces coherent electron wave functions in QDs. The coherence removes QD discrete energy level degeneracy in the chain and bunches the split sublevels into one energy band.
The electron tunneling probability P is a parameter that characterizes transparency of the barrier located on the ultrathin interface between Ge QDs to electrons, with $0 < P < 1$, where the limit $P = 0$ refers to total opacity of QD-QD interface, i.e., $V = \infty$, and $P = 1$ refers to completely transparent interface, i.e., $V = 0$; V being the barrier height. The transparency parameter (tunneling probability) exponentially decays with the square root of barrier height so that $V \sim (\ln P)^2$. Since tunneling probability is reciprocal to the resistivity, we can attain experimentally the transparency parameter by using nanoscale analysis of electrical resistivity, for instance, by Scanning Kelvin Probe. Semi-transparent interface (oxide) layer between Ge QDs at angle $n_\varphi \varphi_0$, where n_φ is an integer, adds an angular dependent potential barrier $V(\varphi)$ in Schrodinger Equation for the angular component of the wave function,

$$V(\varphi) = \frac{\hbar^2}{m^*} \frac{1}{4\varphi_d} (\ln P)^2 \sum_{n_\varphi}^{2\pi/\varphi_0} \delta(\varphi - n_\varphi \varphi_0) \tag{4}$$

where φ_d is the effective thickness (in angular units) of the barrier layer thickness between Ge QDs; and $\delta(\varphi - n_\varphi \varphi_0)$ is a delta-function. Such semi-transparent potential barrier yields discontinuity at angles $n_\varphi \varphi_0$ at the interface between Ge QDs so that the logarithmic derivative of the wave function jumps by $(\ln P)^2 / 2\varphi_d$,

$$\frac{\partial}{\partial \varphi} \Phi(\varphi_0 + 0) - \frac{\partial}{\partial \varphi} \Phi(\varphi_0 - 0) = \frac{1}{2\varphi_d} (\ln P)^2 \Phi(\varphi_0) \tag{5}$$

In the above equation, the angular term of the wave function, $\Phi(\varphi)$, is invariant with respect to φ_0 angle (rotation about the pore axis shown in Fig.17). Such invariance leads to Bloch theorem, that is mathematically expressed as follows:

$$\Phi(\varphi + \varphi_0) = \exp(i n_\varphi \varphi_0) \Phi(\varphi) \tag{6}$$

where, n_φ is limited, however, as compared to Kronig-Penney model.
The continuity of wave function at φ_0, $\Phi(\varphi_0 + 0) = \Phi(\varphi_0 - 0)$, and the jumping of its derivative at the interface combined with the above equations yield a secular equation. The roots of this equation is a set of discrete values for the angular quantum number m:

$$\cos\left(n_\varphi \varphi_0\right) = \cos\left(m\varphi_0\right) + \frac{1}{4\varphi_d m}\left(\ln P\right)^2 \sin\left(m\varphi_0\right) \tag{7}$$

where the integer n_φ is within the interval $0 < n_\varphi \le 2\pi/\varphi_0$.
The hole wave function must swiftly decay for $r_1 < r$ region (from Ge/Si interface into Si bulk material) since the finite potential barrier of the energy band offset at Ge/Si interface confines holes within the chain of Ge QDs,

$$\Psi\left(r,\varphi,z\right) = \left[\exp\left(i\varphi m\right) + a\times\exp\left(-i\varphi m\right)\right] K_m\left(\kappa r\right)\exp\left(\kappa r_1\right)\sin\left(k_z z\right) \tag{8}$$

where $\kappa^2 = \frac{2m_{Si}^*(\Delta E_v - E)}{\hbar^2}$,

- m_{Si}^* is the effective mass of holes in Si,
- $K_m\left(\kappa r\right)$ is the order m modified Bessel function of second kind, which is also called MacDonald function, and
- ΔE_v is the energy band offset in the valence band.

The boundary condition requires continuity of the wave functions and their derivatives at Ge/Si interface that is at $r = r_1$. Application of these requirements to equations (3) and (8) yields secular equation that determines a set of discrete energy levels for confined holes

$$\frac{K_{m+1}\left(\kappa r_1\right)}{K_m\left(\kappa r_1\right)} - \frac{k}{\kappa}\frac{Y_{m+1}\left(k r_1\right)J_m\left(k r_2\right) - J_{m+1}\left(k r_1\right)Y_m\left(k r_2\right)}{Y_m\left(k r_1\right)J_m\left(k r_2\right) - J_m\left(k r_1\right)Y_m\left(k r_2\right)} = 0 \tag{9}$$

where the radial momentum (wave number k) is related to the hole energy E as $E = \hbar^2 k^2 / 2m^*$; and the angular quantum number m must be determined from equation (7).

3.3.4.3.2 For electrons

The chain of Ge QDs incrusted in PS allows electron confinement, for instance, if the Si/Ge interface is opaque for electron transport. However, such confinement becomes a virtual "confinement" in case of ultrathin oxide layer that electrons easily pass through so that the electron wave functions expand from the chain into Si. Such interface adds a radial potential barrier in Schrodinger Equation for the radial component of the wave function

$$V\left(r\right) = \frac{\hbar^2}{m^*}\frac{1}{4r_d}\left(\ln P\right)^2 \delta\left(r - r_1\right) \tag{10}$$

r_d is the effective thickness of the barrier layer thickness between Ge QDs and Si wall. Such semi-transparent potential barrier yields discontinuity at radius r_1 at the interface between Ge QDs and Si wall so that the logarithmic derivative of the wave function jumps by $\left(\ln P\right)^2 / 2r_d$.
The continuity of electron wave function requires the continuity for both angular and radial components of the wave functions. Hence for the radial component one obtains the following boundary condition:

$$\begin{aligned}&\left[Y_m\left(k r_1 + b\right)J_m\left(k r_2\right) - J_m\left(k r_1 + b\right)Y_m\left(k r_2\right)\right] \\ &= C_{mk}\left[Y_m\left(k r_1\right)J_m\left(k r_2\right) - J_m\left(k r_1\right)Y_m\left(k r_2\right)\right]\end{aligned} \tag{11}$$

where the angular quantum number m is obtained from equation (7), as indicated above. The discontinuity of the electron wave function derivatives at the interface r_1 adds one more condition for recognition of two unknown parameters, b and C_{mk}, in equation (2) for the electron wave function:

$$k\left[Y_m'(kr_1+b)J_m(kr_2)-J_m'(kr_1+b)Y_m(kr_2)\right]=$$
$$C_{mk}\times\left\{k\left[Y_m'(kr_1)J_m(kr_2)-J_m'(kr_1)Y_m(kr_2)\right]+\frac{(\ln P)^2}{2r_d}\left[Y_m(kr_1)J_m(kr_2)-J_m(kr_1)Y_m(kr_2)\right]\right\} \quad (12)$$

3.3.4.4 Results and discussion

3.3.4.4.1 Virtual "confinement" in conduction band

The continuity of the electron wave functions and the derivative jump at the interface (i..e, at r_1) determine two secular equations. Hence two integration constants, b and C_{mk}, of electron wave function can be determined. Whereas equation (9) yields discrete roots and thus discrete momentum wave numbers k, equations (11) and (12) yield continuous values of b (integration constant) and C_{mk}, as functions of radial momentum wave number k (and hence electron energy E). Therefore, energy solutions for electron localization can exist within the chain of QDs, as equations (11) and (12) do not impose any restriction on the allowed values of electron momentum k.

In the case of total opacity of Ge/Si interface, $P\approx 0$, equation (7) yields integer angular quantum number m, and equation (12) that yields the following simpler equation $Y_m(kr_1)J_m(kr_2)-J_m(kr_1)Y_m(kr_2)=0$, which is very close to $\sin(kr_1-kr_2)=0$. It gives a discrete set of energy states shown in Fig. 18 for electrons confined in the chain of Ge QDs.

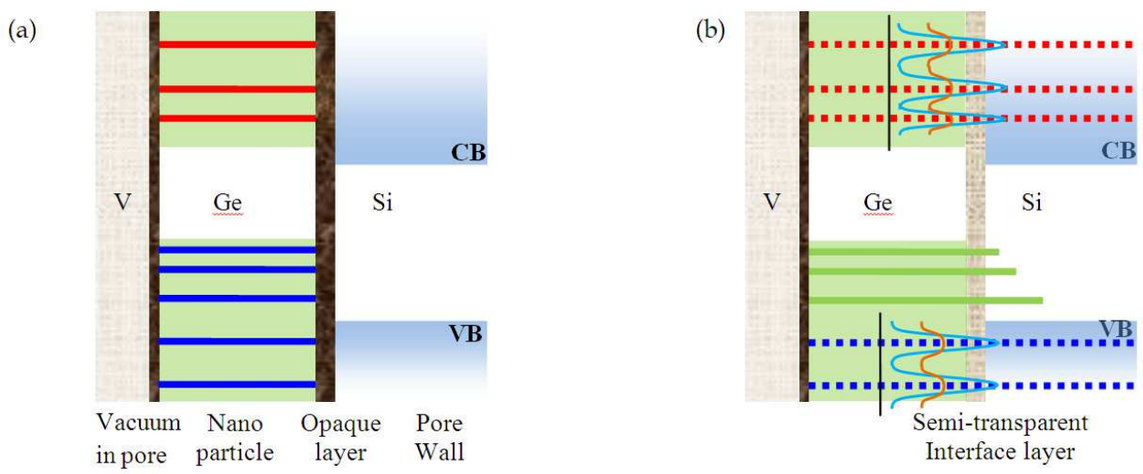

Fig. 18. Schematic diagram of energy bands for the chain of identical QDs clinging onto cylindrical pore walls in porous silicon.

$$E=\frac{\pi^2\hbar^2 n_k^2}{2m^*(r_1-r_2)^2} \quad (13)$$

where n_k =1, 2, 3,.... Here n_k is the principal quantum number for electron confinement along the radius of the QD chain. The principal quantum number is related to the radial momentum *k*.

Schematic diagram of energy bands for the chain of identical QDs clinging onto the cylindrical inner walls of a pore in PS. Green regions represent band edges, separating the Ge bandgap. Red lines are the resonant electronic states in conduction band and the blue lines are the hole confined blue lines are the hole confined states in the valence band. The textured bar is semi-transparent oxide.

Energy levels associated to confined states in Ge dots, with an interface opaque to charge carrier transfer, are visible in Fig. 18 (a), as bleu lines for holes and red for electrons. For comparison the host material energy bands are added. Likewise, Fig.18 (b) shows these levels extending to the silicon (virtual states) due to the semi-transparent interface QD-Si walls. Insets show charge carrier probability related to QD virtual states as a function of the transparency of interface layer barrier (bleu is for higher transparency value). In the case of semi-transparent Ge/Si interface, $0 < P < 1$, solutions of the secular equations (11) and (12) produce a continuous energy spectrum for electrons in the chain of QDs. However, in contrast to electrons in the bulk Si, the amplitude of wave functions is very small in the chain for about all electronic states,

$$\left|C_{mk}\right|_{\min} \approx \frac{\pi\left(2n_k+1\right)r_d}{\left(\ln P\right)^2\left(r_1-r_2\right)} \tag{14}$$

Only for resonant energies that are close to values given by equation (13), the amplitude of electron wave functions is large in the chain

$$\frac{1}{\left|C_{mk}\right|^2} \approx \frac{8r_d^2 m^* E_R}{\hbar^2\left(\ln P\right)^2} + \frac{\left(\ln P\right)^4}{4r_d^2}\left(r_1-r_2\right)^2\left(\sqrt{\frac{E}{E_R}}-1\right)^2 \tag{15}$$

where $E_R = \dfrac{\pi^2\hbar^2 n^2}{2m^*\left(r_1-r_2\right)^2}$ and the width at half-maximum is $\Delta E \approx \dfrac{\sqrt{2}\pi^3\hbar^2 n^3 r_d^2}{m^*\left(\ln P\right)^4\left(r_1-r_2\right)^4}$.

Figure 19 shows that ΔE is small (narrow lineshape) with E_R is very high.

It is worth mentioning that the resonance can occur (i) even between distant Ge QDs in the chain and (ii) even in the case of opaque Ge/Ge interface between QDs due to the electronic coupling through the silicon pore walls. Such "virtually confined" electronic states must also promote electron percolation between QDs. The amplitude of the "virtually confined" electronic waves is so large in Ge QDs that the probability to find electron with energy E_R in QDs is huge compared to that in the same QD-size volume of silicon. Such contrast in amplitudes makes difficult electron escape from "virtually confined" resonant states of QDs into Si and makes easy the opposite transitions.

Large amplitude of electron resonance modes increases probability of two low-energy photon absorption in PS because such absorption is proportional to the electron wave function amplitude in the chain of QDs in PS.

3.3.4.4.2 Confinement in valence band

The roots of the secular equation (9) is a set of discrete energy levels E for holes confined in the chain of QDs, $E = \hbar^2 k^2 / 2m^*$. This transcendental equation is the secular equation of the

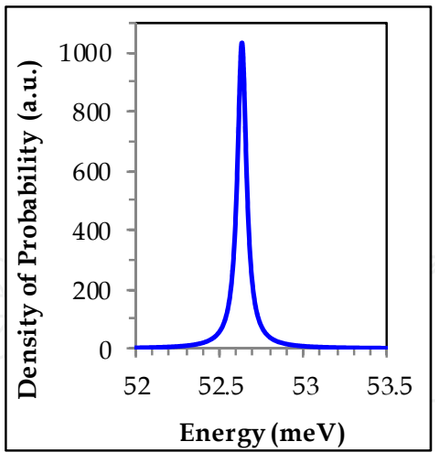

Fig. 19. Square of the amplitude of electron density $|C_{nk}|^2$ as a function of radial momentum kr_1 in the chain of QDs. Interface opacity is $P = 0.5$ and QD size is $r_1 - r_2 = 10\ nm$.

system; it can be solved numerically using a non-linear solver. Approximate roots can be found graphically the zeros of the characteristic function (the term on the left side of the equation).

In the case of opacity interface layer between QDs for hole transport, $P = 0$, each of these levels is n_0 time degenerated; here n_0 is the number of Ge QDs within the chain. However, the degeneracy is removed as the interface transparency increases, $0 < P < 1$. In this case, the discrete energy levels split and give rise to narrow energy bands totaling n_0 electronic states very close in each band.

Because the energy E does not have an explicit dependence on the angular quantum number m, one could conclude that angular confinement of holes would not influence their energy. In fact, k implicitly depends on the angular quantum number m because equation (7) determines allowed values of m for the secular equation (9), which creates implicit dependence of k as well as energy $E = \hbar^2 k^2 / 2m^*$ on the angular quantum number m. Crossing of the blue curve with energy axis in Figure 20 (a) shows the solution of equation (9) for m=400. The red dashed lines point out the solution of the secular equation (9) for m within the range 10 to 100 for which the curve overlap. One can see that the lowest value of energy E for $m = 400$ increases up to 33 meV compare to that for $m = 10$ and $m = 100$. Calculation has showed that this result depends on the ratio $(r_1 - r_2)/(r_1\varphi_0)$ of QD radial to angular sizes.

Solution of Equation (7) yields a series of discrete values for angular quantum numbers m for each integer n_φ from the interval $0 < n_\varphi \le n_0$, where $n_0 = 2\pi/\varphi_0$. Figure 20 (a) displays this series of angular quantum numbers m as a function of the integer n_φ for the chain of $n_0 = 100$ Ge QDs inserted in a cylindrical pore of PS. In the case of opaque interface layer between the chain of QDs, calculation results in the same m for all integer values of n_φ, which means n_0-fold degeneration of these confined electronic states, $n_0 = 100$. The red dashed line in Figure 20 (a) displays such solution. Even a weak transparency of the interface layer between QDs breaks degeneration and splits of the degenerate states into narrow energy bands. The width of the bands depends on the interface transparency P of the interface layer between QDs. The blue curve in Figure 20 (a) displays the removing of n_0-fold degeneracy and the splitting into the band in the case of interface transparency P

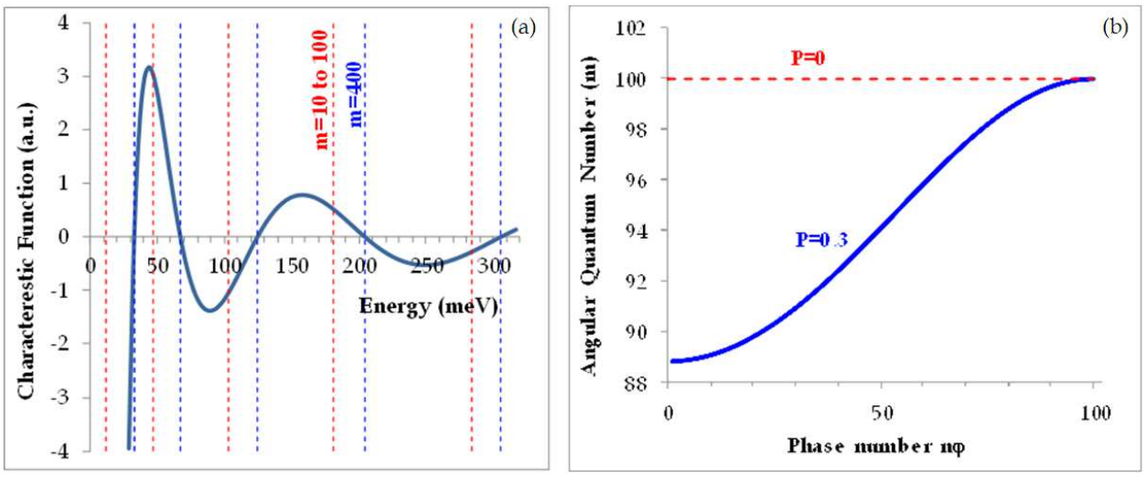

Fig. 20. (a) Eigenvalues obtained by solving the secular equation (9) graphically. Red lines point to the roots for the m within 10 to 100 range, in which case the eigenvalues are about the same. Blue curve is the characteristic function of the secular equation for $m = 400$.
(b) Splitting of degenerated confined states in the chain of Ge QDs clinging onto pore walls in PS. Null intra-chain transparency (between QDs) to electrons shows non-dependence of the angular momentum quantum with the phase number. This results in a full degenerescence of the energy levels.

equal to 0.3. Noteworthy, the angular quantum numbers m of those n_0-split states are not integer, $n_0 = 100$, as all 100 states cluster within narrow interval of close numerical values $88.5 \le m \le 100$.

Calculations show that the reduction of QD angular size φ_0, which increases the number n_0 of QDs in the chain, $n_0 = 2\pi/\varphi_0$, increases the numerical value of the first m in the sets of allowed angular quantum numbers. Because the first m determines the order of the Bessel functions in equation (9) the reduction of φ_0 may also increase the energy of ground confined state in the valence band of Ge QDs. Though the bands are still confined in the valence band of the chain, they also extend into the Si walls because the wave functions decay into Si along a hole tunneling depth. Transparency P of the interface layer between the Si wall and the chain of Ge QDs determines the depth of the band extension into silicon. The salient features of the split bands are (i) within the silicon bandgap, and (ii) extend from the chain of Ge QDs into the Si walls. Both are very favorable features for two low-energy absorption and IB operation of such bands in PS.

3.3.4.4.3 Density of states

The density of states (DOS) in the chain of Ge QDs is the sum of delta-functions over all discrete energy levels, $\rho(E) = \sum_{n_k \ge 1} 2\delta\left(E - E_{n_k}\right)$. The splitting into bands removes degeneration of states and also transforms the DOS $\rho(E)$ in the chain of Ge QDs. The transformation depends on the transparency P of the interface layer between QDs. Figure 21 (a) displays evolution of the density $\rho(E)$ of states per *pore* per *meV* in the confined band split by the interface layer transparency, $P = 0.14$, in the chain of n_0 QDs, ($n_0 = 100$) all QDs are considered identical. The Ge QD thickness, which is along the pore radius,

$\delta r = r_1 - r_2$ is varied from $5nm$ to $3nm$. All QDs have the same angular size $r_1\varphi_0$ .equal to $2\pi r_1/n_0$. The area limited by dark green trapezoids is the same, $n_0 = 100$, for all δr thicknesses because initially all confined states have the same n_0-fold degeneration. The base of green trapezoids is the widths of the split bands. Figure 21 (a) shows that reduction of the QD thickness δr increases the density $\rho(E)$ of states and reduces the width of the split bands. The dashed red and green lines illustrate such dependence on the radial thickness δr of QDs for two ultimate split energies in the band, which refer to angular quantum numbers $m = 88$ and $m = 100$, respectively.

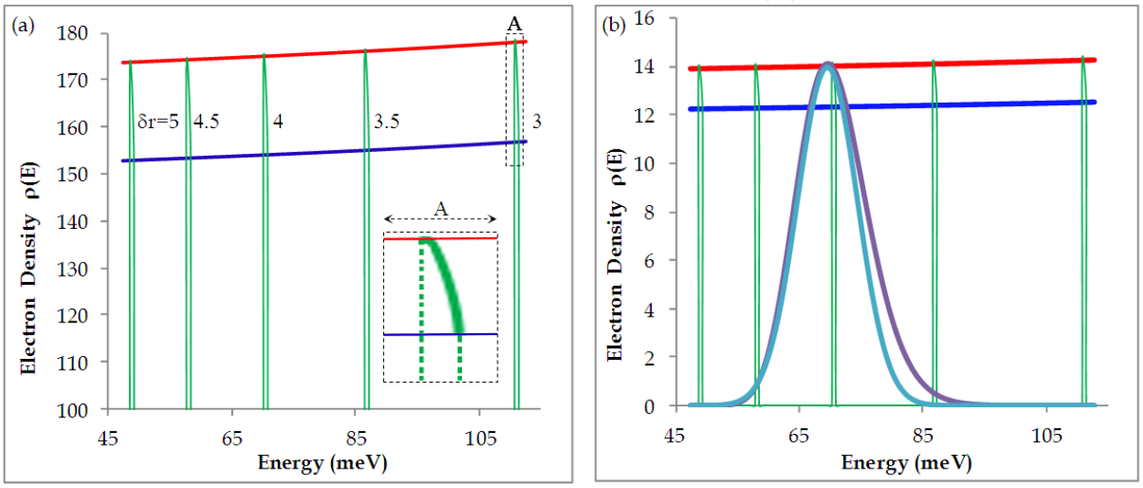

Fig. 21. (a) Density of confined states $\rho(E)$ (per *pore* per *meV*) in the split band. The inset is an enlargement of the electron density function of energy for nanodot thickness of 3 % of the pore radius. (b) The density of confined electronic states (per *pore* per *meV*) in PS for a QD normal size distribution.

The density of the band states in PS could be large as it is related to the large density of pores. The appearance of energy band with large density of confined electronic states in PS is very important for efficient IB solar cell applications. Evidently, properties and potential of such IB in PS are highly sensitive to the ability of controlling the size distribution of Ge QDs in PS (Sun et al., 2005; Abd Rahim et al., 2010).

Fabrication of Ge QDs in PS inevitably imbeds different size Ge QDs into the pores. Depending on the dispersion their contribution in the density of electronic states in PS becomes a weighted function of the dispersion. In case of Gaussian (normal) distribution of QD thicknesses (radial parameter), the weight function is $\left(1/\sqrt{2\pi\sigma^2}\right)\exp\left[-(r-r_{10})^2/\left(2\sigma^2\right)\right]$, where r_{10} is the mean thickness and σ is the dispersion of QDs. The dark blue curve in Figure 21 (b) displays the density of confined states in PS for normal distribution of QD thicknesses that $r_{10} = 4nm$ and $\sigma = 0.2nm$. The scale of dark green trapezoids is reduced by 0.08 times for eye guide. One can compare two cases and see that even a small dispersion of QD thicknesses in PS, $\sigma = 0.2\,nm$, expands the distribution of states into a wider energy band. The dispersion also reduces 0.08 times the maximal

DOS, which occurs at the mean thickness, $r_{10} = 4nm$. Note that the area under both curves are the same as the total number n_0 of Ge QDs in the chain.

The density $\rho(E)$ of states shown in Figure 21 (b) is a skewed Gaussian; compare with the normal distribution (Gaussian) shown in blue (fitted to the actual DOS). The peak of the fitted DOS is at 62.5 *meV* and the dispersion is 4.85 *meV*.

4. Summary

As most of the third generation photovoltaic devices and the used materials are nanostructured, quantum phenomena turn out to be effective. Hence, they must be taken in consideration when designing such devices. Likewise, light-matter interaction quantum processes can be directly or indirectly involved in the photoelectric effect; they are numerous and complex. Therefore, as we move into nanoscale photovoltaic materials targeting higher efficiency solar cells, these processes need extreme attention.

In this chapter we put the emphasis on detailed mechanisms involved in the photoelectric effect in semiconductors. Silicon great relevance for technology calls for more research to overcome the main hurdle related to its indirect bandgap. Also the involvement of a wide range of fundamental processes in connection to the photoelectric effect makes the discussion on Si and Ge indirect semiconductor interesting for this quantum mechanics chapter complexity. We have reviewed fundamental quantum processes taking place in electron and phonon systems in a semiconductor, independent of the device consideration. We then have discussed those systems in nanostructured materials and heterostructures. We have evoked and used (**E-k**) energy-momentum dispersion relationship in semiconductors, which is essentially of quantum origin, results in different energy gaps and electron effective masses. These vary with the symmetry points in semiconductor energy-momentum space. Most of the quantum processes involved in the photoelectric effect, which are initiated by photon absorption, have been reviewed in relation to the energy band structure of the absorber. Hence, we described the quantum nature of photon absorption and photon emission processes resulting in electron-hole generation and recombination in solids.

Because photon energy is transferred in a discrete form, generated photoelectron has higher energy than it may contribute in the produced electricity. We assessed the major losses in solar cells and have singled out those that have quantum bearings. We discussed various mechanisms for carrier generation and recombination with consideration of the energy exchange and the net conversion. This led to discussing the thermalization, photon recycling aspect occurring in reality in the course of photoelectric effect processes etc. Ultimately, we went through the net produced charge carrier subsequent to photon absorption or charge carrier injection and recycling.

We went through the three main conceptual limitations of solar energy conversion, namely: the second law of thermodynamics, the Shockley-Queisser, and the Luque-Marti limits. It is necessary to take into account these three physical limitations if one is to exploit every available portion of photon energy in the solar spectrum. Thereafter, we have looked at the physics of multispectral devices known to give the highest efficiency records and compared it to the more recent concept proposed by Luque. For that matter, we analyzed the energy band structure of materials that have an Intermediary Band. We then have compared two published schemes for the generation of IB materials and their use in optoelectronic and photovoltaic devices. For the first, the IB is located within the electronic p-n junction, while

for the second, which is a newer concept, the IB material is outside that region. The first appeared to practically turn QDs intended to enable the IB in recombination centers that degrade the conversion efficiency instead of increasing it. In the newer scheme, the IB material is located outside the electric field within the depletion region, with the intention of preventing charge carrier recombination. In that case the IB material is simply an absorber with an enhanced absorption in the energy range lower than the bandgap. In essence, this is in line with the goal of using IB in photovoltaic devices, that is to generate additional photocurrent while the conventional photocurrent resulting from the VB-CB band to band transitions remains intact.

After clarification of the photoelectric effect fundamental aspects and the routes for high efficiency solar cells, one of the author's approaches to make IB enabled materials was unveiled. It is based on the functionalization of porous silicon with Ge quantum dots. The IB enabled PS solar cells is a new idea that the author (Karoui & Kechiantz, 2011) has been studying experimentally and theoretically through modelling. The author's modeling methodology of the intermediate band enabled porous silicon for solar cells was then summarized and some results have been discussed.

A simple model of QDs necklace-like chain of identical QDs has been put together. The chain is constituted of a regular distribution of QDs, all dots clinging into the pores of PS material. The Schrodinger equation was solved for a single chain in a circular pore, in the effective mass approximation. We realized that this system is described by two essential parameters i.e., angular momentum and radial momentum quantum numbers. We determined the hole and electron wave functions and energy levels in the chain of QDs. The energy spectrum of such system appeared to depend on transparency of the interface layer between the chain of QDs and Si wall, and on transparency of the interface layer between QDs in the chain.

We have discussed the interface transparency factors. For that purpose we looked at published literature about the composition of oxide cap layers, the physical properties such as dangling bond, the layer formation and decomposition, etc. We have analysed the interface layer material properties for Ge-QD-chain/Si-walls material system. The interface layers of such system is a solid solution of SiO_2, GeO_2, and GeO oxides. The composition, structure, and thickness of the interface, which determine its transparency, depend on fabrication technology. To be noted, if the interface is totally impermeable to electrons, the width at half-maximum ΔE of the electron wave function vanishes and the electron energy spectrum becomes discrete. Remarkably, even for extremely small values of interfaces transparency, electrons from the cavity walls (i.e., host material) spill over the QDs, which results in a continuous component in the energy spectrum. However, most wave functions of such electrons vanish in the Ge QDs, while some resonant modes grow large. These resonant electronic states are "virtually confined" in QDs, they easily accommodate electrons from pore walls of PS.

We then showed that Ge QDs introduce a narrow band of evanescent electronic states that being confined in the chain material; these states also expand into the pore wall of the host material due to the quantum mechanics tunnelling. In case of valence band in Ge(QD)/Si(wall) material system, the narrow band of evanescent states is aligned with the Si bandgap, which gives them a potential for being effective within the IB enabled PS material. The density of such IB states is an important parameter for efficient performance of IB PS solar cells. We have shown that IB density in PS may be large if the thickness of pore

walls is comparable with electron tunnelling depth into PS. Our calculation has revealed that the discrete energy spectrum of confined holes is highly sensitive to electron transparency of the interface layer between QDs in the chain. While an opaque interface layer, which completely separates QDs from each other, yields a degenerated discrete spectrum. A semi-transparent interface layer removes such degeneration and widens the discreet spectrum into a narrow IB.

In the valence band of Ge QDs, the confined states induce narrow energy bands lined within the Si bandgap. These Ge valence band states spill over and decay in the PS, whereas conduction band resonant electronic states extend from Si into the Ge QDs, even if the interface between Ge and Si is semi-transparent for charge carriers. The salient features of the split bands are (i) lining up with the silicon band gap, and (ii) extension from the chain of Ge QDs into the Si walls. Both are essential properties for the absorption of two low-energy photons via the IB. Such properties are desirable for Ge QD modified PS based solar cells. The chosen material system put forward an electronic structure that is efficient with respect to electron transitions induced by low energy photons.

Because QDs grown in PS inevitably have a random size distribution, their contribution into the density of electronic states is a weighted function of the size (thickness and breadth) dispersion. We have calculated the density of IB electronic states in PS and studied the size dispersion effect on the DOS in IB. Our study has shown that Gaussian size distribution of QD yields a non-Gaussian distribution of density of states in IB, this result is owing to the quantum confinement in the chain of QDs.

5. Acknowledgment

This material is based upon work supported by the US Department of Defense, Contract Number: W91CRB-10-C-0321. The authors are indebted to Dr Sondes Karoui for discussing the manuscript.

6. References

Arenas, M.C.; Hu, H.; Antonio, del Rıo J.; Salinas, O.H., (2008). Photovoltage & J-V features of porous silicon, *Rev. Mex. Fıs.* Vol.54, (5) pp. 391–396

Abd Rahim, A.F.; Hashim, M.R. & Ali, N.K. (2010). Study of Ge embedded inside porous silicon for potential MSM photodetector, *Microelectronics International, Vol.* 27, No. 3, pp. 154–158

Afanas'ev, V.V.; Fedorenko, Y.G.; & Stesmans, A. (2005). Interface traps & dangling-bond defects in (100)Ge/HfO2, *Appl. Phys. Lett.* , Vol. 87, 032107

Ai, N.; Sul, O.; Begliarbekov, M.; Song, Q.; Kumar, K.; Choi, D. S.; Yang, E.-H. & Strauf, S. (2010). Transconductance & Coulomb Blockade Properties of In-Plane Grown Carbon Nanotube Field Effect Transistors, Nanosci. Nanotechnol. Lett, , Vol. 2, (2) pp. 73-78

Aleiner, I.L.; Brouwer P.W. & Glazman, L.I. (2002). Quantum effects in Coulomb blockade, *Physics Reports,* Vol. 358, pp. 309-440

Alguno, A.; Usami, N.; Ohdaira, K.; Pan, W.; Tayanagi, M. & Nakajima, K. (2006). Influence of stacked Ge isl&s on the dark current–voltage characteristics & the conversion efficiency of the solar cells, *Thin Solid Films,* Vol. 508, No. 1-2, pp. 402 – 405

Aroutiounian, V.; Petrosyan, S.; Khachatryan, A. & Touryan, K. (2001). Quantum dot solar cells, J. *Appl. Phys.,* Vol. 89, pp. 2268-2271

Baumgartner, K.; Holländer, B.; Carius, R.; Ahrens, B.; Angelov, O.; Sendova-Vassileva, M.; Dimova-Malinovska, D. & Schweizer, S. (2010). Photon down-conversion in Terbium(III)-doped thin dielectric films & fluorozirconate glasses for thin film solar cells, Proc. SPIE 7725, 77250T; doi:10.1117/12.853939

Boucaud, P.; Le Thanh, V.; Sauvage, S.; Debarre, D. & Bouchier, D. (1999). Intraband absorption in Ge/Si self-assembled quantum dots, *Appl. Phys. Lett.,* Vol. 74, pp. 401–403

Boucaud, P.; Le Thanh, V.; Sauvage, S.; Debarre, D. & Bouchier, D. (1999). Intraband absorption in Ge/Si self-assembled quantum dots, Appl. Phys. Lett., Vol. 74, pp. 401

Denker, U.; Stoffel, M.; Schmidt, O.G. & Sigg, H. (2003). Ge hut cluster luminescence below bulk Ge band gap, *Appl. Phys. Lett.,* Vol.82, (3), pp. 454-456

Derivaz, M.; Noe, P.; Rouviere, J.L.; Buttard, D.; Sotta, D.; Gentil, P. & Barski, A. (2002). Epitaxial growth of germanium dots on silicon (001) surface covered by a very thin dielectric layer, Materials Science & Engineering B89, pp. 191–195

Dimoulas, A.; Tsipas, P.; Sotiropoulos, A. & Evangelou, E. K. (2006). Fermi-level pinning & charge neutrality level in germanium, *Appl. Phys. Lett.* Vol.89, pp. 252110 -252112

Dziewior, J. & Schmid, W. (1977). Auger coefficients for highly doped & highly excited silicon, *Appl Phys Lett,* Vol. 31(5) pp. 346

Fromherz T.; Koppensteiner E.; Helm M.; Bauer G.; Nutzel J. F. & Abstreiter G. (1994). Hole energy levels & interband absorption in modulation-doped Si/Si1-xGex multiple quantum wells, *Phys Rev B* vol.50, (20), pp. 15073-15085

Fukatsu, S.; Sunamura, H.; Shiraki, Y. & Komiyama, S. (1997). Phononless radiative recombination of indirect excitons in a-Si/Ge type-II quantum dot, Appl. Phys. Lett. Vol. 71, pp. 258

Green, M.A. (1984)Limits on the open-circuit voltage & efficiency of silicon solar cells imposed by intrinsic Auger processes, *IEEE Trans on Electron Devices ED*, Vol. 31, (5) pp. 671-678

Green, M.A. (1998). Solar Cells, *in Modern Semiconductor Device Physics* Ed S M Sze, Wiley, New York

Guyot-Sionnest, P.; Shim, M.; Matranga, C. & Hines, M. (1999). Intraband relaxation in CdSe quantum dots, *Phys Rev,* Vol.60, (4) R2181-R2184

Halsall, M.P.; Dunbar, A.D.F.; Shiraki, Y.; Miura, M. & Wells, J-P R. (2004). Hole confinement & dynamics in d-doped Ge quantum dots, J. Luminescence, Vol.108, pp. 329–332

Handbook of Photovoltaic Science & Engineering, ed Luque, A.; Hegedus, S., Wiley, 2003

Hao, P.H.; Hou, X.Y.; Zhang, F.L. & Wang, X. (1994). Energy band lineup at the porous-silicon/silicon heterointerface measured by electron spectroscopy, *Appl. Phys. Lett.* , Vol. 64, (26) pp. 3602

Hovis, J. S.; Hamers, R. J. & Greenlief, C. M. (1999). Preparation of clean & atomically flat germanium(001) surfaces , *Surface Science*, Vol.440, L815–L819

Jolley, G.; Lu, H.F.; Fu, L.; Tan, H.H. & Jagadish, C. (2010). Electron-hole recombination properties of In0.5Ga0.5As/GaAs quantum dot solar cells & the influence on the open circuit voltage, *Appl Phys Lett*, Vol.97, pp. 123505

Karoui, A.; Kechiantz, A. Sensitization of Porous Silicon with Germanium Quantum Dots for Up-Conversion of Low Energy Photons via Intermediate Band for Third

Generation Solar Cells, (2011) ECS Transactions *Photovoltaics for the 21st Century*, Eds. M. Tao, C. Clayes, L. Deligiani, Vol. 41, Issue (4), pp. 53-60.

Karoui, A. Analysis of Formation Mechanisms of Porous Silicon for Photovoltaics Using Nanoscale Raman Scattering and Photoluminescence, Proc. Conf. Symposium (B) Photovoltaic Materials and Manufacturing Issues, October 4 – 7, 2010, Denver, CO.

Karoui, A.; Zhang, H. Porous Silicon Formation and Photoluminescence Decay Analysis, Proc. (2010) Conf. Symposium E8 - Photovoltaics for the 21st Century 6, The 218th Electrochemical Society Meeting - Las Vegas, Oct. 10 - 15, 2010.

Karoui, A.; Zhang, R., Rozgonyi, G. A.; &, Ciszek, T. (2001) Silicon Crystal Growth and Wafer Processing for High Efficiency Solar Cells and High Mechanical Yield, Proc. Conf. NCPV, NREL /CP-520-31057, Lakewood, CO, 14-17 Oct. 2001.

Kechiantz, A.M.; Kechiyants, H.M. & Kocharyan, L.M. (2007). band Alignment & Conversion Efficiency in Si/Ge Type-II Quantum Dot Intermediate band Solar Cells, *Nanotechnology*, Vol. 18, pp. 5401

Kita, K.; Takahashi, T.; Nomura, H.; Suzuki, S.; Nishimura, T. & Toriumi, A. (2008). Control of high-k/germanium interface properties through selection of high-k materials & suppression of GeO volatilization, Appl. Surf. Sci., Vol. 254, pp. 6100

Konle, J.; Presting, H. & Kibbel, H. (2003). Self-assembled Ge-isl&s for photovoltaic applications Physica E, Vol. 16, pp. 596

Kurtz, S.; Johnston, S., & Branz, H.M. (2005). Capacitance-spectroscopy identification of a key defect in N-degraded GalnNAs solar cells Appl. *Phys. Lett.*, Vol. 86, pp. 113506

Lee, C. H.; Tabata, T.; Nishimura, T.; Nagashio, K.; Kita, K. & Toriumi, A. (2009). Ge/GeO2 Interface Control with High-Pressure Oxidation for Improving Electrical Characteristics, *Appl. Phys. Express 2*, 071404

Lee, C. & Wang, K. L. (1994). Electron intersubband absorption in Ge/Si1−xGexquantum-well structures grown on Si (001) substrate, *Appl. Phys. Lett.* , Vol. 64, pp. 1256

Lin, L.; Xiong, K. & Robertson, J. (2010). Atomic structure, electronic structure, & band offsets at Ge:GeO:GeO2 interfaces, *Appl. Phys. Lett*, Vol. 97, pp. 242902

Luque, A. & Marti, A. (1997). Increasing the efficiency of ideal solar cells by photon induced transitions at intermediate levels, *Phys. Rev. Lett.* , Vol. 78, pp.5014

Luque, A. & Marti, A. (2010). The Intermediate band Solar Cell: Progress Toward the Realization of an Attractive Concept, Adv. Mater, Vol.22, pp.160–174

Luque, A.; Marti, A.; Stanley, C.; Lopez, N.; Cuadra, L.; Zhou, D.; Pearson, J.L. & McKee, A. (2004). General equivalent circuit for intermediate band devices: Potentials, currents & electroluminescence J. Appl. Phys. , Vol. 96, pp. 903-909

Marti, A.; Cuadra, L. & Luque, A. (1999). Quantum dot super solar cell, Proc. Conf. on Sobre Dispositivos Electronicos Madrid pp. 363-366

Marti, A.; Cuadra, L. & Luque, A. (2000) Quantum dot intermediate band solar cell, Proc. 28th IEEE Photovoltaic Specialist Conf. (Fairbanks, AK, 2000) pp.940-943

Matsubara, H.; Sasada, T.; Takenaka, M. & Takagi, S. (2008). Evidence of low interface trap density in GeO2/Ge metal-oxide-semiconductor structures fabricated by thermal oxidation, *Appl. Phys. Lett.* , Vol. 93, 032104

Meyer, T.; Klemenc, M. & Von Kanel, H. (1999). Surface electronic structure modifications due to buried quantum dots, *Phys Rev B* , Vol.60, (12), R pp. 8493-8496

Miyazaki, T. & Fukatsu, S. (1999). Diminished photoluminescence polarization due to exciton ionization in strained Si1−xGex/Si(001)quantum wells, *Appl. Phys. Lett.* , Vol. 75, pp.3962

Nozik, A.J. (2002). Quantum dot solar cells Physica E 14 115

Prabhakaran, K. & Ogino, T. (1995). Oxidation of Ge(100) & Ge(111) surfaces: an UPS & XPS study, *Surface scienc* , Vol. 325, pp. 263

Prabhakaran, K.; Maeda, F.; Watanabe, Y. & Ogino, T. (2000). Thermal decomposition pathway of Ge & Si oxides: observation of a distinct difference, *Thin Solid Films,* Vol. 369, (1-2) pp. 289-292

Schaffler, F. (1997). High-mobility Si & Ge structures, *Semicond. Sci. Technol.* , Vol. 12, pp.1515–1549

Schmidt, O.G. & Eberl, K. (2000). Photoluminescence of monolayer to submonolayer thick Ge1−zCz on Si (111), *Semicond. Sci. Technol.* Vol. 15, pp. 399–402

Seok, J. H. & Kim, J. Y. (2001). Electronic structure & compositional interdiffusion in self-assembled Ge quantum dots on Si(001), *Appl. Phys. Lett* , Vol.78, (20), 3124-3126

Shockley, W. & Queisser, H.J. (1961). Detailed Balance Limit of Efficiency of p-n Junction Solar Cells, *J Appl Phys,* Vol. 32, pp. 510-519

Sinton, R. A. & Swanson, R. M. (1987). Recombination in Highly Injected Silicon, IEEE Trans on Electron Devices ED-34(6) pp.1380-1389

Sun, K. W.; Kechiantz, A.; Lee, B. C. & Lee, C. P. (2006). Ultrafast carrier capture & relaxation in modulation-doped InAs quantum dots, *Appl. Phys. Lett.,* Vol. 88, 163117

Sun, W.; Kherani, N.P.; Hirschman, K.D.; Gadeken L.L. & Fauchet P.M. (2005). A three-Dementional porous silicon p-n-diode for betavoltaics & Photovoltaics, Adv. Mater. 17, 1230-1233

Svantesson, K.G. & Nilsson, N.G. (1979) The temperature dependence of the Auger recombination coefficient of undoped silicon, *J Phys C,* Vol.12, pp.5111

Sze, S. M.; Irvin J. C. (1968). Resistivity, Mobility, and Impurity Levels in GaAs, Ge, and Si at 300 K, Solid-State Electron., Vol. 11, pp. 599–602

Tersoff, J.; Teichert, C. &. Lagally, M. G, (1996). Self-Organization in Growth of Quantum Dot Superlattices, *Phys. Rev. Lett.,* Vol. 76, pp. 1675–1678

Tsakalakos, L. (2008). Nanostructures for photovoltaics, *Materials Science & Engineering R* , Vol. 62 pp. 175–189

Wahnon, P. & Tablero, C. (2002). Ab initio electronic structure calculations for metallic intermediate band formation in photovoltaic materials, *Phys. Rev. B,* Vol.65, pp.165115

Wang, S. K; Kita, K.; Lee, C. H.; Tabata, T.; Nishimura, T.; Nagashio, K. & Toriumi, A. (2010). Desorption kinetics of GeO from GeO2/Ge structure, *J. Appl. Phys.,* Vol. 108, pp. 054104

Wang, S.K.; Kita, K.; Nishimura, T.; Nagashio, K. & Toriumi, A. (2011). Isotope Tracing Study of GeO Desorption Mechanism from GeO2/Ge Stack Using 73Ge & 18O, Jpn. *J. Appl. Phys.,* Vol. 50 04DA01

Weber, J.R.; Janotti, A.; Rinke, P. & van de Walle, C.G. (2007). Dangling-bond defects & hydrogen passivation in germanium, *Appl. Phys. Lett.,* Vol. 91, pp. 142101

Yu, M.; Walukiewicz, W.; Wu, J.; Shan, W.; Beeman, J.W.; Scarpulla, M.A.; Dubon, O.D. & Becla, P. (2003). Diluted II-VI Oxide Semiconductors with Multiple band Gaps, *Phys Rev Lett.*, Vol. 91 pp.246403

Zibik, E.A.; Grange, T.; Carpenter, B.A.; Porter, N.E.; Ferreira, R.; Bastard, G.; Stehr, D.; Winnerl, S.; Helm, M.; Liu, H. Y.; Skolnick, M.S. & Wilson, L.R. (2009)Long lifetimes of quantum-dot intersublevel transitions in the terahertz range, *Nature Materials,* Vol. 8, pp. 803 - 807

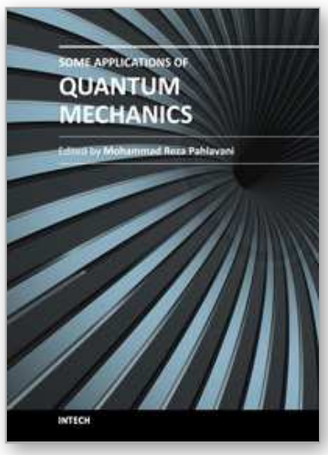

Some Applications of Quantum Mechanics

Edited by Prof. Mohammad Reza Pahlavani

ISBN 978-953-51-0059-1
Hard cover, 424 pages
Publisher InTech
Published online 22, February, 2012
Published in print edition February, 2012

Quantum mechanics, shortly after invention, obtained applications in different area of human knowledge. Perhaps, the most attractive feature of quantum mechanics is its applications in such diverse area as, astrophysics, nuclear physics, atomic and molecular spectroscopy, solid state physics and nanotechnology, crystallography, chemistry, biotechnology, information theory, electronic engineering... This book is the result of an international attempt written by invited authors from over the world to response daily growing needs in this area. We do not believe that this book can cover all area of application of quantum mechanics but wish to be a good reference for graduate students and researchers.

InTech Europe
University Campus STeP Ri
Slavka Krautzeka 83/A
51000 Rijeka, Croatia
Phone: +385 (51) 770 447
Fax: +385 (51) 686 166
www.intechopen.com

InTech China
Unit 405, Office Block, Hotel Equatorial Shanghai
No.65, Yan An Road (West), Shanghai, 200040, China
中国上海市延安西路65号上海国际贵都大饭店办公楼405单元
Phone: +86-21-62489820
Fax: +86-21-62489821

IntechOpen